Nano Research
2023, 16(12): 13419–13433

ISSN 1998-0124 CN 11-5974/O4
https://doi.org/10.1007/s12274-023-5564-7

Review Article

Synthesis and application of green solvent dispersed organic semiconducting nanoparticles

Siwen Zhang[1,2], Hong Zhang[2] (✉), Shuo Yang[3], Xin Zhang[1,2], Shilin Li[4], Liqing Huang[1,2], Ya-nan Jing[4], Linge Xiao[2], Yuan Zhang[4], Bing Han[5] (✉), Jia-jie Kang[1] (✉), and Huiqiong Zhou[2] (✉)

[1] *China School of Engineering and Technology, China University of Geosciences (Beijing), Beijing 100083, China*
[2] *CAS Key Laboratory of Nanosystem and Hierarchical Fabrication, National Center for Nanoscience and Technology, Beijing 100190, China*
[3] *Beijing Tingrun Membrane Technology Development Co., Ltd., Beijing 101102, China*
[4] *School of Chemistry, Beihang University, Beijing 100191, China*
[5] *The Department of thoraciccardio surgery, PLA Rocket Force Characteristic Medical Center, Beijing 100088, China*

Received: 16 December 2022 / **Revised:** 9 February 2023 / **Accepted:** 10 February 2023

ABSTRACT

Organic photovoltaic semiconductors have made significant progress and have promising application prospects after decades of development. When compared with traditional semiconductors, the solution method for preparing photovoltaic semiconductors shows the advantages of low cost and convenient preparation. However, because of the extremely poor solubility of the polymers used to prepare semiconductors, toxic solvents must be used when using the solution method, which has significant negative effects on the environment and operators and severely limits its development prospects. Organic nanoparticles (NPs), on the other hand, can avoid these issues. Because NPs are typically water or alcohol-based, no toxic solvents are used. Furthermore, NPs have been used in organic solar cells, hydrogen catalysis, organic light-emitting diodes, and other fields after nearly two decades of development, and their preparation methods have been developed. We describe the preparation, optimization, and application of NPs in photovoltaic semiconductors in this review.

KEYWORDS

nanoparticle, organic semiconductor, miniemulsion method, nanoprecipitation method, surfactant

1 Introduction

Organic semiconductors have caught the attention of scientists since the 1940s. Most polycyclic aromatic compounds can combine with halogens to form semiconducting charge-transfer complex salts with conductivities ranging from 0.1 to 1 $S \cdot cm^{-1}$ [1]. With the efforts of Heeger, MacDiarmid, Shirakawa et al., the conductivity increased to 10^4–10^5 $S \cdot cm^{-1}$ in the 1970s [2]. Conductive organic semiconductor materials doped with polyacetylene won the Nobel Prize in Chemistry in 2000. As a result, the study of organic semiconductors has piqued the interest of many academics since 2000. Organic semiconductors, unlike traditional inorganic semiconductors, can be prepared by solution methods and have unique advantages such as strong designability [3], low fabrication cost [4], light weight [5], and flexibility [6, 7]. However, during the preparation process, solution treatment is required [8], but the organic semiconductors are mostly non-polar or weakly polar molecules, and their solubility in non-toxic and harmless solvents is very poor. In the preparation of high-performance organic semiconductor devices, although solvent-free mechanochemical methods such as ball milling technology are used to avoid the use of toxic and harmful solvents in the synthesis process [9–12], vacuum evaporation, physical vapor transportation, and other methods can be used to reduce the harm of toxic and harmful solvents [13]. On the one hand, these methods have certain limitations, such as ball milling technology does not have advantages in the synthesis of asymmetric molecules and macromolecules. The reaction conditions need to be further optimized and the product yield of the reaction is low; vacuum evaporation and physical vapor transmission methods involve high temperature, and will form oxygen by-products that affect semiconductor performance. On the other hand, the operation method is complex and not conducive to large-scale production. The solution treatment method is simpler to operate, has a flexible preparation process, is suitable for large-area production, and shows great advantages [14, 15]. But the organic semiconductors are mostly non-polar or weakly polar molecules, and their solubility in non-toxic and harmless solvents is very poor. So when using the solution-processed method, good crystal morphology and molecular arrangement are particularly important. In order to obtain good results, the material must be completely dissolved, which requires the use of a large number of toxic solvents, which seriously limits the industrial production of organic semiconductors. Figure 1 shows the toxicity and solubility of common solvents [16–18]. The abscissa in the figure only represents the quantitative standard of the harm of solvents to human health, and the data is derived from the methods of environmental, health, and safety (EHS) assessment and life cycle

Address correspondence to Hong Zhang, zhanghong@nanoctr.cn; Bing Han, phanbing2008@126.com; Jia-jie Kang, kangjiajie@cugb.edu.cn; Huiqiong Zhou, zhouhq@nanoctr.cn

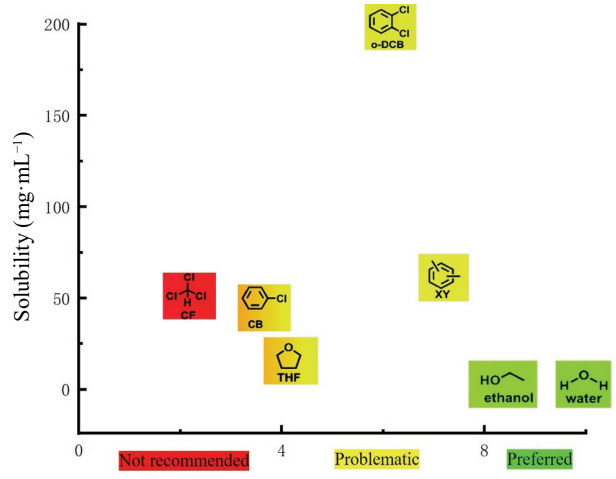

Figure 1 Illumination of toxicity and solubility of common solvents used in organic semiconducting. The solubility was obtained by Bright Walker et al. according to the solubility of solvent to $PC_{71}BM$ [17]. The green, yellow, and red colour codes represent preferred, problematic, and not recommended solvents, reference from green solvent processed organic electronic devices [16].

assessment (LCA) (ISO, 1997). However, to judge whether the solvent is recommended for use, it is not only necessary to consider the harm to human health, but also the harm to the environment, the difficulty of causing the harm, and other factors. Therefore, EHS and other institutions put forward nine factors that need to be considered comprehensively (including release potential, fire/explosion, reaction decomposition (safety hazards), irritation, chronic toxicity, acute toxicity (health hazards), air hazards, water hazards, and environmental persistency (environmental hazards)), each of which has its own quantitative criteria, and finally make a comprehensive evaluation. According to the quantity and degree of hazards involved in different solvents, the quantitative rating is generally divided into three levels, namely preferred, problematic, and not recommended solvents [16, 19]. The ordinate reflects the solubility of solvent to semiconductor materials. We take solvent of [6,6]-phenyl C_{71} butyric acid methyl ester (PC71BM), a classic semiconductor material, as an example [17].

In view of this, researchers have tried different ways, such as the use of halogen-free solvents [20], the design of polymer molecules that can be treated with green solvents [21], the selection of suitable green solvents [22], and the use of nanoparticles (NPs) manufacturing processes [23]. The classic organic semiconductor solution approach commonly uses solvents such as chloroform (CF) and chlorobenzene (CB) [18]. These solvents cause substantial harm to the human body after evaporation, and even have carcinogenic effects. Due to the existence of halogenated chemicals, the release in the atmosphere will destroy the ozone layer and generate acid rain, and the loss to the ground will continue to accumulate, harming soil and groundwater [24]. Non-halogenated solvents such as tetrahydrofuran (THF) and 1,2-dimethylbenzene (O-XY), although are less hazardous, however, still have some hazards that cannot fundamentally solve the problem. Thus, the molecular design aims to change the structure of semiconductor materials to make these materials have good solubility in green solvents (water, ethanol, etc.). For different semiconductor material architectures, the solubility can be successfully increased by adding terminal functional groups or functional side chains to the alkyl chain of the polymer [25, 26]. The inclusion of polar groups or polar side chains can also boost solubility [27]. The primary chain of many polymers is relatively strong, which limits their solubility, however, introducing an alkyl chain or olefin linkage into the main chain can effectively boost the solubility [28]. Hydrophilic terminal groups are added to the end of the small molecule alkyl chain to generate a small molecule electrolyte, thereby enhancing the solubility [29]. Replacing the terminal functional groups of the original molecules and replacing the original symmetrical functional groups with asymmetric ones can improve the solubility of molecules in non-polar organic solvents [30, 31]. Although the process of molecular design can alleviate the solubility problem to a certain extent, it will raise the difficulty of synthesizing materials and degrade the performance of materials. Moreover, the performance of organic semiconductors prepared by semiconductor molecules obtained by molecular engineering is less competitive than that of semiconductor molecules dissolved in toxic solvents. Some scholars avoid the use of harmful solvents by looking for green solvents with similar solubility to harmful solvents, or mixing green solvents and harmful solvents to reduce the use of harmful solvents [32, 33]. Due to the limitations of semiconductor materials, it is difficult to find a suitable solvent. The approach of synthesizing organic semiconductor materials into NPs and distributing them in alcohol or water in the form of colloids seems to be more suitable for greening. The synthesis of polymers or small compounds with poor solubility into NPs does not need to consider the problem of low solubility [34].

In this review, we discussed the synthesis of green solvent-dispersed organic semiconductor nanoparticles, as well as their application in semiconductor devices and the key factors affecting device performance. The focus is on the miniemulsion process and nanoprecipitation method for NPs preparation, and the four influencing factors are the use of surfactants, ultrasonic treatment, solution concentration, and annealing treatment. Finally, we update the current status of NPs development in organic photovoltaics (OPVs), photocatalytic hydrogen evolution, organic light emitting diodes (OLEDs), and organic field effect transistors (OFETs).

2 Synthesis of nanoparticles

Nanoparticles are typically defined as solid colloidal particles with diameters ranging from 10 to 1000 nm. NPs can be prepared in a variety of ways which fall into two broad categories [35, 36]. The first type requires pre-polymerization, such as solvent evaporation, nanoprecipitation, salting out, and dialysis, whereas the second type is prepared directly by polymerizing monomers using classical polymerization or polymerization reactions, such as emulsion polymerization, miniemulsion polymerization, and microemulsion polymerization. However, because the polymers used to synthesize NPs are extremely insoluble, they must be dissolved in organic solvents, and the presence of surface active agents and stabilisers during the synthesis process has a significant impact on the performance of semiconductor devices. As a result, the majority of NPs used in photovoltaic semiconductors today are prepared by miniemulsion and nanoprecipitation. The specific steps are detailed further below.

2.1 Miniemulsion method

Miniemulsions are very small stable emulsions developed by Chou et al. [33]. It is proposed that resistance to Ostwald ripening and collisional coalescence be overcome in order to stabilise the microemulsion. Surfactants and mechanical stirring forces are thus required to fabricate and maintain the stability of microemulsions. Mechanical agitation causes droplet size distribution in a heterogeneous fluid containing surfactants. Surfactants provide some stability to the droplets, allowing them to overcome the Laplace force between them. The magnitude of the Laplace force is proportional to the size of the droplets. When

mechanical stirring disperses the droplets to a certain extent and the surfactant's stability is insufficient to balance the Laplace force between the droplets, the small droplets will eventually combine to form large droplets, reaching an equilibrium state [37]. Indeed, the size of the droplet has been reported to be proportional to the stability scale, which is a good reflection of the aforementioned formation process [38]. Some researchers believe that the osmotic pressure of the trapped species and the droplet's Laplace pressure resolve the evolution of the emulsion, and that these surfactants provide electrostatic or steric stability to the droplet. This does not contradict the preceding theory. In 2002, Landfester et al. first fabricated NPs solutions of semiconducting polymers in chloroform and water by the miniemulsion method. During the next 20 years of research, the application of miniemulsions in organic semiconductors has risen dramatically [39].

The preparation of organic semiconductor NPs by miniecroemulsion method can be divided into four main processes. First of all, organic semiconductor is dissolved in good solvents (such as CF and O-XY), and surfactants are dissolved in water. Then the two solutions are mixed in a certain proportion to form a coarse emulsion, as shown in step (a) in Fig. 2. After that, the mixed solution is stirred or sonicated to apply strong mechanical force to form a mini-emulsion, as shown in step (b) in Fig. 2. Then, the organic solvent is removed by stirring or pumping in an inert gas to obtain an aqueous solution of the miniemulsion, as shown in step (c) in Fig. 2. After that, in order to obtain the miniemulsion solution we need, we usually use centrifugal filtration, concentration, and other methods to remove excess surfactant and increase the concentration of NPs.

The final step of surfactant removal is also extremely important. Since the surfactant is an impurity in the NPs, and the surfactant is not conductive, it will inevitably affect the performance of the NPs to prepare the semiconductor. Details of the effects of surfactants are provided later in Section 3.

2.2 Nanoprecipitation

Fessi initially suggested the solvent replacement approach, commonly referred to the nanoprecipitation method, in 1989 [40]. Three components make up the nanoprecipitation preparation: polymer, polymer solution, and non-polymer solvent. The non-polymer solvent and the solvent in the polymer solution should be soluble in each other well. The technique is based on the interfacial deposition of polymers following the displacement of an organic solution by water or alcohol-miscible semi-polar solvent, such as THF. Polar solvents are completely miscible in the non-solvent phase, causing the polymer to reach a state of supersaturation in the organic solution, resulting in phase separation as the polymer becomes completely insoluble in the mixture to form NPs. This happens when the good solvent phase is added to the majority of the poor solvent phase. The miscibility and solubility criteria between the two phases must be met during the nucleation process [35]. Surfactants can be used to effectively regulate the size of NPs [41]. The process of polymer precipitation under spontaneous dispersion of polymer solutions is known as nanoprecipitation. The method is made simpler and there is less chance of contaminating the NPs when premade polymers are used [42]. The process of encapsulating known as nanoprecipitation is thought to be straightforward, repeatable, affordable, low-toxic, and effective [41].

The nanoprecipitation approach eliminates the need for a harsh miniemulsion preparation step by fabricating NPs from premade polymers. According to Fig. 3, there are three basic steps in the fabrication of NPs for organic semiconductors utilizing the nanoprecipitation method. The nucleation procedure is shown in Fig. 3(a). In order to form the NPs dispersion system, the organic semiconductor solution is first mixed in a certain proportion in a poor solvent (such as water and alcohol). As shown in Fig. 3(b), when stirring, the organic solution is gradually dropped into the poor solvent and kept for a period of time under the condition of applying mechanical force to obtain smaller NPs. In order to disperse NPs in water or ethanol, it is necessary to pump inert gas to remove the excess organic solvent. Occasionally, surfactants are used to generate NPs through nano precipitation, so a centrifugal filtration step may be required to remove any additional surfactants.

The nanoprecipitation approach is more straightforward than

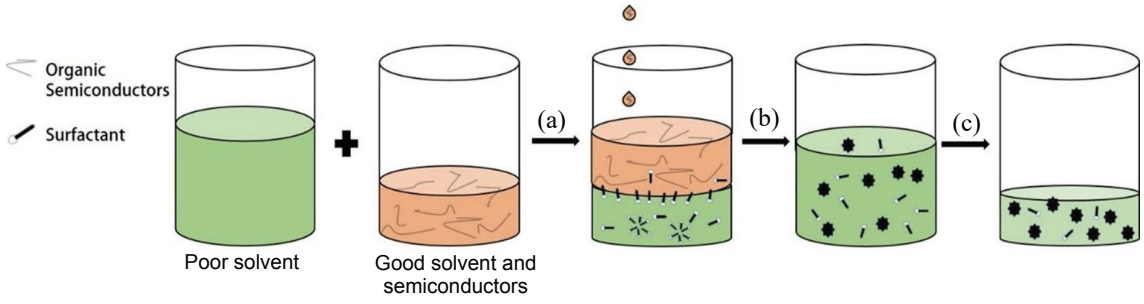

Figure 2 Techniques for the preparation of miniemulsions: (a) sonication to form miniemulsions, (b) followed by a solvent evaporation step to form NPs, and (c) concentrate the dispersion and remove excess surfactant by dialysis or centrifugal dialysis. Reproduced with permission from Ref. [43], © American Chemical Society 2021.

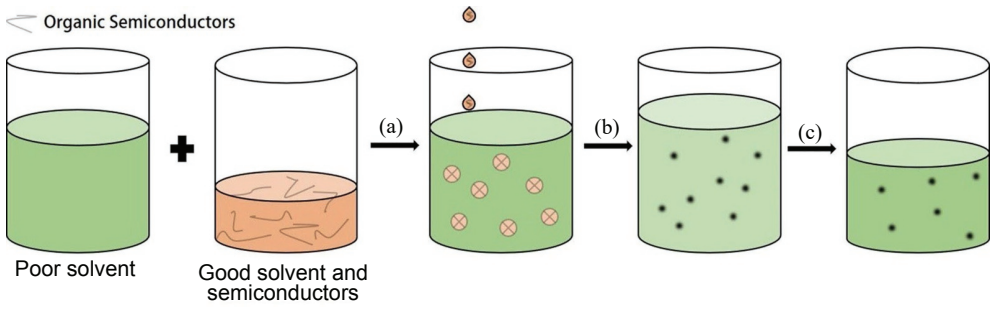

Figure 3 Nano-precipitation preparation technology: (a) The organic semiconductor dissolved in the organic solvent is added dropwise to the water with stirring. (b) Since solvent and non-solvent are miscible, a solvent displacement step occurs, resulting in NPs formation (through nucleation and growth). (c) Removal of the organic solvent to obtain a dispersion in an aqueous medium. Reproduced with permission from Ref. [43], © American Chemical Society 2021.

the miniemulsion method for the fabrication of organic semiconductor NPs. The synthesis processes are analogous, despite the fact that the nucleation principle is different, and as a result, the precautions are also similar. The main difference is the choice of good solvents. For the miniemulsion method, good and poor solvents are completely incompatible, and NPs nucleation is a two-step process. First, after mixing the solvents, small droplets containing semiconductor materials are produced when external forces are applied. After removal of good solvents, the semiconductor materials in small droplets aggregate into NPs [44]. For nanoprecipitation, good and poor solvents can be miscible, and nucleation of NPs takes only one step. Semiconductor materials are directly displaced and precipitated to form NPs during solution mixing. The size of NPs is affected by the addition of mechanical external force. NPs nucleate before the removal of good solvents [45]. However, as shown in Fig. 4, there is a big gap between the NPs structures prepared by the two methods. The NPs prepared by the miniemulsion method have a shell–core structure [46], while the NPs prepared by nanoprecipitation are more uniformly mixed particles without obvious shell–core distribution [47].

3 Factors affecting the quality of nanoparticles

Although the synthesis process of organic NPs has been developed and the applications have been explored for more than a decade, in many cases, the quality of the synthesized NPs is too poor to manufacture desired semiconductor devices and undesired semiconductor devices due to improper handling during application. In this section, some influencing factors and suggestions for improving the process will be systematically described.

3.1 The effect of surfactants

In the preparation of NPs by the miniemulsion method, after the emulsion reaches a stable state by applying shear force, it needs to be homogenized, and the surfactant molecules play an extremely important role in the homogenization.

3.1.1 Choice of surfactant

When making NPs using miniemulsions, surfactants are extremely important for producing NPs of the right size. Surfactants can assist in achieving greater solids and more stable dispersions when utilising nanoprecipitation [48]. The selection of surfactants is crucial since the use of surfactants carelessly have the opposite effect. In order to discover a surfactant suited for polymer NPs, Cho et al. employed an intolerant naphthalene diimide (PNDI)-2-(2-(thiophen-2-yl)vinyl)thiophene (TVT) as the solute and fabricated a colloidal dispersion system using a range of surfactant aqueous solutions. Figure 5 displays the surfactants that are tested [49]. Ionic surfactants with large aromatic hydrophobic groups and nonionic surfactants have produced very large particles in preliminary experiments that are hundreds of microns in size. Colloidal particles are steadily dispersed when surfactants with linear chains and charged hydrophilic groups are used. Two anionic surfactants, sodium dodecyl sulfate (SDS) and sodium dodecyl benzene sulfonate (SDBS), and two cationic surfactants, dodecyl trimethyl ammonium bromide (C_{12}TAB) and benzyl dimethyl dodecyl ammonium bromide (BDAB), were tested. According to the critical micelle concentration and hydrophile lipophilic equilibrium (HLB) value of the surfactant, the reaction time and solute concentration of the miniemulsion in each surfactant were optimized. The hydrodynamic diameter and polydispersity index of colloidal particles prepared by these four

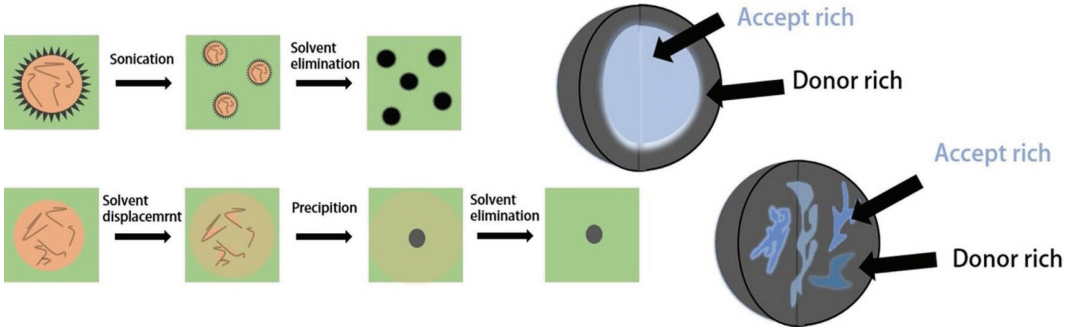

Figure 4 Comparison of NPs prepared by microemulsion or nanoprecipitation. Reproduced with permission from Ref. [43], © American Chemical Society 2021.

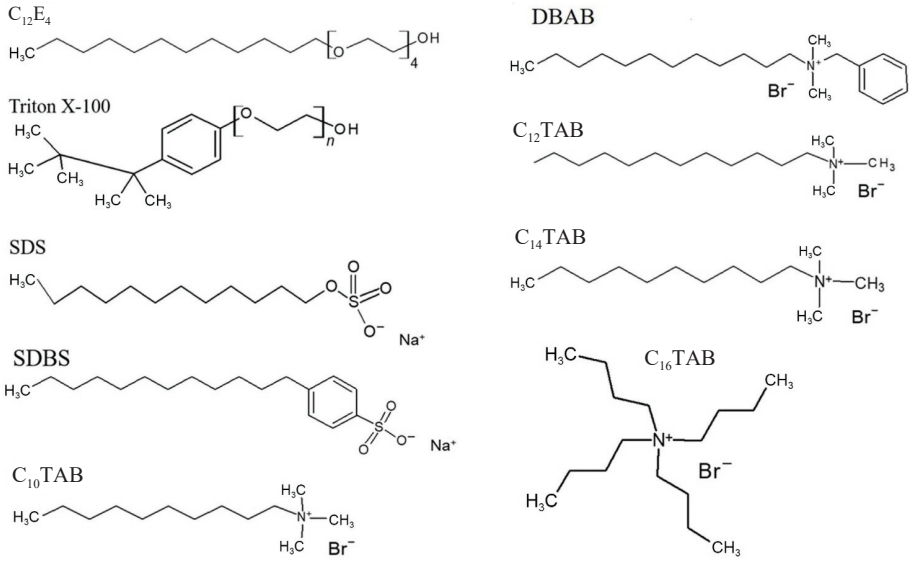

Figure 5 Tested instant noodle active agent structure.

anionic surfactants were analyzed. The four surfactants are effective. The colloidal films of C_{12}TAB and BDAB had smooth and continuous film morphologies, while the colloidal films of SDS showed discontinuous films made up of large local clusters with a certain roughness. The discontinuous and rough morphology of SDS-based colloidal membranes can be attributed to excessive surfactant micelles. The equation of depletion contact energy U_c is provided for the fact that huge clusters are fabricated through interparticle flocculation before the agglomeration process

$$U_c = -\left(\frac{1}{4}\right)\pi nKT\sigma_2\sigma_1^2$$

where n is the micelle concentration, K is the Boltzmann constant, T is the temperature, σ_1 is the micelle diameter, and σ_2 is the particle diameter. The smoother the film formation, the smaller the U_c. Here, a summary of four criteria for choosing a surfactant is provided:

(1) The emulsifying effect of ionic surfactants with large aromatic hydrophobic groups and nonionic surfactants is not ideal.

(2) To minimize U_c, the concentration of surfactant cannot be too high.

(3) The residual surfactant can be effectively removed.

(4) When the surfactant concentration is higher than the critical micelle concentration (CMC), the aggregates formed have a high degree of order, so the longer alkyl chain is more advantageous.

Surfactants also affect the ratio of donor to acceptor in NPs. Because of the different affinity of surfactants to donor–acceptor when good solvents are removed, they form a shell–core structure, which affects the ratio of donor to acceptor. Jan Kosco et al. used sodium 2-(3-thienyl) ethoxybutylsulfonate (TEBS) with a similar affinity for PTB7-Th and EH-IDTBR to replace SDS with a large affinity difference. The optimal ratio of PTB7-Th and EH-IDTBR was increased from 10:90 to 30:70, which greatly improved the donor-to-acceptor ratio and the efficiency of the device [50].

3.1.2 *Surfactant removal*

Although the use of surfactants in the fabrication of NPs cannot be avoided, their non-conductivity will have an impact on the functionality of the resulting semiconductor devices. Surfactants in excess or remaining in NP films might change the morphology of the film, as shown in Figs. 6(a)–6(c). The negative effects of residual surfactants on devices cannot be ignored. The conventional approach involves stabilizing the NPs and then removing them using repeated centrifugal filtering, washing, or dialysis. According to Cho et al., nonionic surfactants fabricate a surfactant layer on top of the deposited film due to poor nonionic interactions, which can be washed away to neutralise the effect [51]. Cho et al. efficiently removed the surfactant SDS from the film by annealing it at a high temperature of 270 °C after employing poly[2,5-bis(3-tetradecylthiophen-2-yl)thieno[3,2-b]thiophene] (PBTTT) colloid to fabricate organic thin-film transistors [52]. Andrew Stapleton et al. found that high-temperature annealing can get rid of surplus surfactant when they studied how annealing temperature affects NPs films [53]. For the nonionic surfactant F127, Xie et al. developed an effective surfactant removal technology, as seen in Fig. 6(e), due to the temperature-sensitive CMC of F127, it is converted to linear F127 in water of 0 °C. Therefore, the colloidal dispersion was rapidly cooled to 0 °C and multiple centrifugal filtrations were conducted after the acceptor material aggregated into stable NPs. It can be seen that the residual amount of F127 cleaned at 0 °C is significantly less than that of other surfactants by contrasting the zeta potential of the NPs dispersions after cleaning with F127, SDS, and dodecyl trimethyl ammonium bromide (DTAB) at room temperature. With a 7.5% conversion efficiency, the PBQ-QF:ITIC NPs fabricated using this approach were successful in fabricating OPV devices.

3.2 Effects of annealing

Because the NPs differ from the substance that is completely dissolved in the solvents, the surface morphology has significant

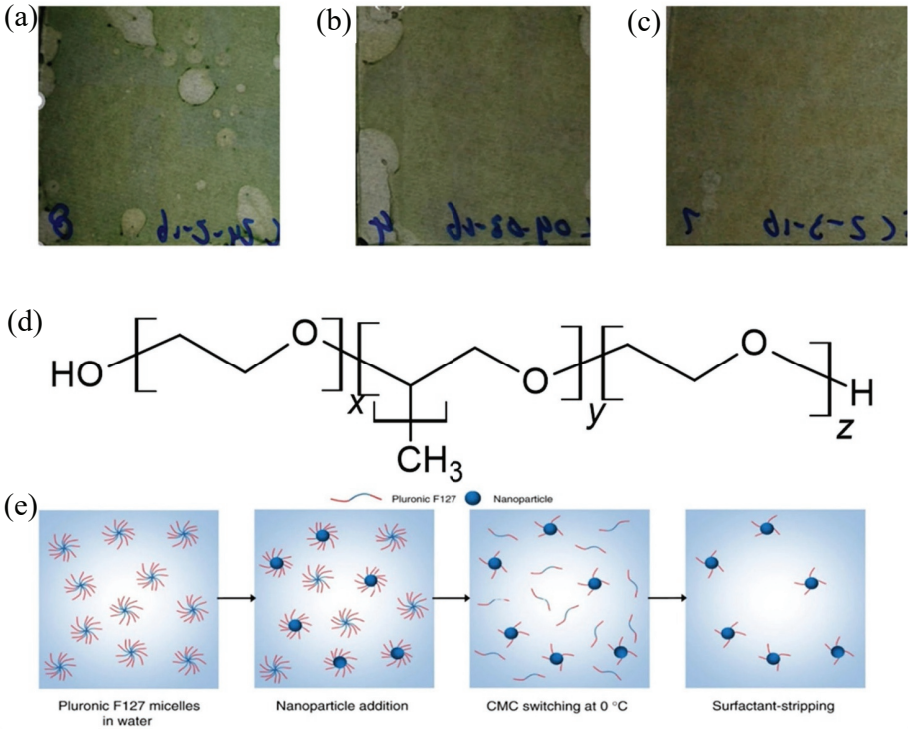

Figure 6 Spin-coated active layer images of (a) high concentration, (b) low concentration, and (c) medium concentration SDS. Reproduced with permission from Ref. [54], © American Chemical Society 2017. (d) Molecular formula of F127. (e) Flowchart for removal of F127. Reproduced with permission from Ref. [53], © Xie, C. et al. 2018.

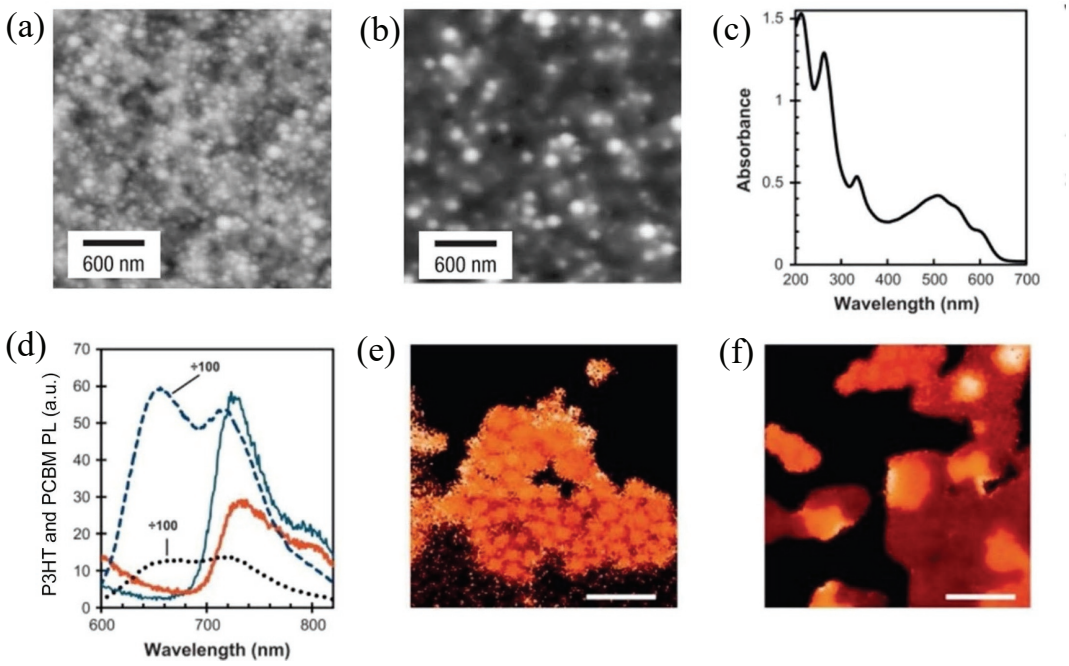

Figure 7 (a) Scanning electron microscopy (SEM) image of m-LPP film before annealing and (b) SEM image after annealing. Reproduced with permission from Ref. [55], © Nature Publishing Group 2003. (c) UV–Vis spectra, (d) PL spectra, (e) composition of P3HT:PCBM STXM before annealing, and (f) composition of P3HT:PCBM STXM after annealing picture. Reproduced with permission from Ref. [56], © Elsevier B.V. 2012.

flaws after the NPs are employed to produce a thin film. Thus, the impact of the annealing phase assumes critical importance.

Although the surface of the film becomes smoother with increasing temperature, the interfacial area between the two components increases, as shown in Figs. 7(a) and 7(b). Thin films spin-coated with one-component NPs of polymers m-LPP by thomas et al. After annealing, the softer PF11112 had a certain fluidity, which made its size and thickness smaller than m-LPP after film formation [52, 57]. Syahrul Ulum et al. compared NPs-OPV with bulk-heterojunction (BHJ) OPV devices before and after annealing. The conversion efficiency of NP OPV before annealing was higher than that of BHJ OPV [56]. However, after annealing, the conversion efficiency of BHJ devices increased and surpassed that of NP devices after annealing. The conversion efficiency of the NP OPV device decreases instead. Poly(3-hexylthiophene) (P3HT) exhibits an absorption peak at about 500 nm, which indicates the degree of polymer conjugation and demonstrates that P3HT has a significant local ordering in the NPs by the ultraviolet–visible (UV–Vis) spectra of the NP films as shown in Fig. 7(c). Figure 7(d) displays the photoluminescence (PL) spectra of P3HT and phenyl-[6,6]-C_{61}-butyric acid methyl ester (PCBM) films before and after annealing. The reduction of impurities and defects and the increase in interchain contacts during annealing, leading to fewer recombination sites, may be the cause of the fall in PL yield after annealing. Figures 7(e) and 7(f) show the P3HT and PCBM compositions in the NP films before and after annealing by scanning transmission X-ray microscopy (STXM). Clearly, NP had a shell–core structure prior to annealing. A significant phase separation developed after annealing. While the P3HT domain expanded, the PCBM domain's makeup remained mostly intact. NP films subjected to heat treatment may form "over-annealed" structures.

It has been established that reasonable annealing can successfully improve the film morphology and improve the device efficiency, even though annealing may result in "over-annealing" and thus affect device efficiency. The device efficiency for the P3HT:ICBA (ICBA: indene-C_{60} bisadduct) NP-OPV device fabricated by Syahrul Ulum et al. was increased to 2.5% after drying at 110 °C for 3 min and annealing at 150 °C for 15 min [58]. Through X-ray photoelectron spectroscopy (XPS) and other measurements, it has been established that the increased device efficiency is not the result of a change in the film's vertical composition. Instead, after annealing, the film retains its NP structure but loses its shell–core structure, allowing the donor–acceptor to mix more thoroughly. Figure 8 displays the evolution diagram. The drying temperature and annealing temperature were further varied by Natalie P. et al. The device efficiency continued to improve during the drying temperature from 90 to 140 °C. Among them, V_{oc} and J_{sc} have been greatly improved, and the change in fill factor (FF) is not obvious. During the process of increasing the annealing temperature from 140 to 260 °C, the best devices were obtained at 140 and 160 °C [59]. The efficiency drastically declines as the temperature rises above 160 °C. The most likely cause of this is "over-annealing". When the drying and heat treatment temperatures are optimized to produce the best equipment, the morphology of the NPs film becomes smoother, from the initial stage when the NPs structure can be clearly observed to the sintering between the NPs, to the formation of a smooth plane, as shown in Figs. 8(b)–8(d). Comparing the test images from the transmission electron microscopy (TEM) and STXM, the device performance trends are connected to the structural alterations in the NPs films at various annealing and drying temperatures. In the film's initial state, particles with a $PC_{71}BM$-rich core and a TQ_1-rich shell predominate. The $PC_{71}BM$-rich core was mostly unaltered after drying at 110 °C, with a few connections between the TQ_1-rich shells. The connections between the shells of TQ_1 tightened after drying at 140 °C; this tendency continued after drying at 110 °C and after annealing at 140 °C. When zooming in on the TEM image after drying at 140 °C, one is able to see that the path of TQ_1 has essentially developed close to the $PC_{71}BM$ core. Small aggregates formed between the $PC_{71}BM$ cores as a result of total phase separation that happened with an increase in annealing temperature. The $PC_{71}BM$ cores were already bigger and aggregated at the annealing temperature of 260 °C, leading to significant phase separation, as shown in Fig. 8. Therefore, a suitable annealing temperature can enhance the morphology and phase distribution of the film, as well as the limitation of the

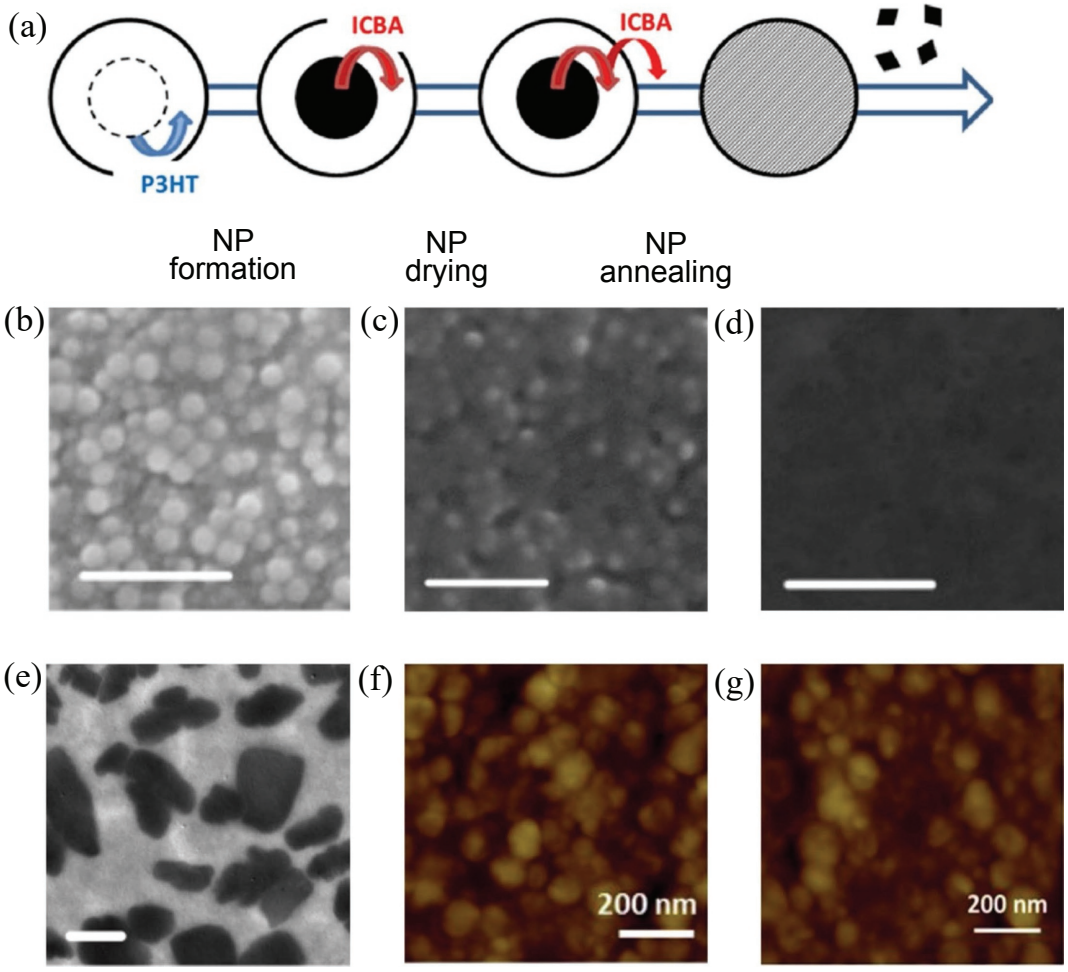

Figure 8 (a) Schematic illustration of NPs evolution during heat treatment. Reproduced with permission from Ref. [58], © Elsevier Ltd. 2013. SEM images of TQ_1:$PC_{71}BM$ NPs films: (b) after annealing at 110 °C, (c) after annealing at 120 °C, (d) annealed at 140 °C, and (e) after annealing at 260 °C. Reproduced with permission from Ref. [60], © Elsevier Ltd. 2015. (f) AFM images of PBDTTPD:$PC_{71}BM$ NPs film after annealing at 180 °C for 4 min and (g) after annealing at 180 °C for 20 min. Reproduced with permission from Ref. [61], © Elsevier B.V. 2016.

shell–core structure, to a certain extent. However, an excessively high temperature will result in significant phase separation and reduce the device's efficiency. Lien et al. increased the device's efficiency by increasing the annealing time after determining the ideal annealing temperature [61]. In PBDTTPD:$PC_{71}BM$ system, when the annealing temperature is changed between 150 and 200 °C, the optimal efficiency of 2% is obtained by annealing at 180 °C for 4 min. When the annealing time is extended to 20 min, V_{oc} is greatly increased and 3.8% efficiency is obtained. Even while the particles are still visible as shown in Fig. 8, the atomic force microscopy (AFM) image reveals that the NPs layer is smoother, demonstrating that increasing the annealing time improves the film morphology.

3.3 Mechanical force

According to the theory of NPs synthesis, the quick mixing of the two phases leads to the nucleation of NPs, and the amount of mechanical force used during mixing will also have an effect. Prunet et al. used stirring rates ranging from 250 to 1000 rpm while maintaining constant initial and final concentrations to compare the synthesis of $PC_{71}BM$ and PCDTBT NPs [62]. The smallest particle size was attained at a stirring speed of 750 rpm. Larger particles are produced when the initial solution is mixed poorly with the aqueous phase at a low stirring speed of 250 rpm due to the insufficient mechanical force that is being provided. Although pure stirring speed at 1000 rpm can result in a greater mixing of the solution with the aqueous phase, the excessive stirring force caused the solvent to form a vortex, which made the dispersion system unstable and led to the development of bigger particles. As a result, sonication, which generates finer mechanical force, is frequently a wise choice. A reliable option for the miniemulsion production of NPs has always been ultrasound. Parrenin et al. fabricated composite NPs of PCDTBT:$PC_{71}BM$ when synthesizing NPs for the fabrication of organic semiconductors [63]. The NPs size was decreased from 140 to 45 nm by increasing the ultrasonic power from 150 to 225 W. Particle size decreased as the sonication time was extended. Parrenin et al. reduced the particle size from 140 to 52 nm and extended the sonication time from 2 to 5 min at a power of 150 W. Ultrasonic power is typically between 30 and 400 W, and ultrasonic time is typically between 1 and 5 min, with a maximum of 2 min, for fabricating NPs for organic semiconductor devices.

3.4 Concentration and solvent ratio

The organic semiconductor solution and poor solvent must be ready in advance of the NPs synthesis. Among these, the solution's concentration plays a significant role in influencing and granulating. By altering the concentration of PDPP5T5T-2:$PC_{71}BM$, Xie et al. were able to produce NPs of various sizes [64]. Particles of 107, 30, 5.2, and 5.0 nm were produced using the starting concentrations of 40, 30, 15, and 10 mg·mL^{-1}, respectively. The size of the NPs will shrink as the fluid concentration drops. Similar results were achieved by Laurie Parrenin et al. They used $PC_{71}BM$:PCDTBT solutions of 5, 30, and 50 mg·mL^{-1}, and under

constant ultrasound time and the same surfactant concentration, they obtained NPs of 30 ± 20, 140 ± 30, and 330 ± 90 nm, respectively. [63] Smaller-size NPs can be produced with a lower initial solution concentration. The particle size of NPs is also somewhat influenced by the ratio of solution to poor solvent. Initial concentrations of 30 and 15 mg·mL^{-1} were utilized by Xie et al., and the proportions of solution to water were 1:3, 1:6, and 1:12. When comparing NPs particle sizes, it is discovered that a higher ratio facilitates the achievement of lower particle size. The characteristics of NPs are also influenced by the organic solvent used. For the preparation of PTNT:$PC_{71}BM$ NPs, Xun et al. utilised chloroform and xylene, respectively. In the same case, the high boiling point of xylene yielded a lower particle size [65].

4 Application of organic semiconductor nanoparticles

After more than ten years of unremitting efforts, the application of NPs in organic semiconductors has made certain progress. It has certain applications in organic solar cells, photocatalytic hydrogen evolution, organic light-emitting diodes, field effect transistors, etc. Among them, applications in OPV and photocatalytic hydrogen evolution have been reported in well-known journals in the industry. The application in OLED and OFETs also has great potential for development. Among them, the water-based NPs have reached a conversion efficiency of 7.5% in OPV.

4.1 In organic solar cells

At present, most applications of organic semiconductor NP are in optical devices. After more than 20 years of development, from fullerene system to non fullerene system, the photovoltaic efficiency of OPV has increased from the earliest 0.004% to 7.5% [53, 55]. The preparation methods also include miniemulsion method and nano precipitation method. At the same time, water-based and alcohol-based NPs were also developed to prepare OPV. Figure 9 reviews the evolution of OPV efficiency for water and alcohol systems. Tables 1 and 2 show the efficiency of aqueous and alcohol-based nanoparticles OPV devices, respectively.

4.1.1 Preparation of OPV devices from aqueous nanoparticles

The original active layer material used for the preparation of OPV is not suitable for the preparation of aqueous-based NPs, and many scholars have developed many new systems suitable for preparing aqueous-based NPs. Figure 10 shows some of the donor and acceptor materials used to manufacture aqueous-based NPs.

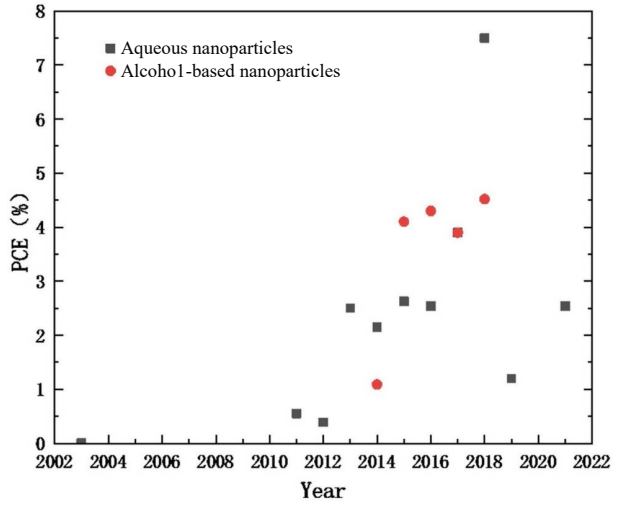

Figure 9 The reported evolution diagram of OPV device efficiency prepared by aqueous and alcohol nanoparticles.

Thomas et al. first synthesized aqueous-based NPs by miniemulsion method, and successfully prepared OPV devices [55]. They synthesized one component NPs through polymer m-LPPP, PF11112, and PMMA, and synthesized mutually enveloped NPs through PFB:F8BT, finally PFB:F8BT NPs obtaining 0.004% conversion efficiency. Following the pairing of the low-bandgap donor materials P1, P2, and P3 with fullerene $PC_{61}BM$, suitable-sized NPs were made using SDS surfactant, and after dialysis, a solid content of 60 mg·mL^{-1} was achieved. After the active agent was fluorinated, knife coating was used to successfully fabricate active layers that were 126 ± 19, 500 ± 25, and 612 ± 22 nm thick [66]. In OPV devices made of PDPPTNT:PC71BM, devices made of NPs films have better exciton diffusion length [67]. The resulting confined form improves exciton collection, and the photocurrent generation is increased compared with comparable BHJ devices. Additionally, by properly annealing the PDPP-TNT:$PC_{71}BM$ NPs active layer, charge transport in the films can be increased. Besides, excessive annealing can result in overall phase segregation within the NP films and hence degrade device performance. The preparation of OPV devices by NPs provides a method to control the initial intrinsic blend morphology, which is independent of the evaporation time during spin coating. This control is related to solvent-free properties of the aqueous dispersions, which is very useful for large-scale manufacturing of the OPV devices. By comparing the transport properties of P(TBT-DPP):ICBA NPs devices with the fitted dark *J*–*V* curves, it is demonstrated that the high density in the nanoparticle structure is responsible for the enhanced charge transport of NPs with close contact between the donor and the acceptor compared to the conventional BHJ devices [s [68]. In the TQ_1:$PC_{71}BM$ NPs system, after annealing at a higher temperature, paths between $PC_{71}BM$ rich NPs cores were developed, which promoted the charge extraction. Moreover, TQ_1 can still maintain its original structure at a higher temperature (up to 85 °C), which effectively improves the stability of OPV devices [60]. Due to PBDTTPD's limited solubility in low boiling point solvents, the NP production technique in the PBDTTPD:$PC_{71}BM$ system was optimised, and chlorobenzene was chosen as a suitable solvent. To get the best power conversion efficiency (PCE) of 3.8%, the as-prepared NPs OPV was annealed at 180 °C for 20 min [61]. The influence of surfactants on the particle size was investigated on the basis of the preparation of NP OPV devices utilising the PDPP5T:$PC_{71}BM$ system [54]. Additionally, PCDTBT:PCDTBT in PC71BM system also requires high boiling point solvent. After being dissolved in O-DCB, NP devices were successfully prepared, and the effect of annealing treatment on conversion efficiency was studied [62, 63, 69]. Additionally, NPs devices were made in the PDPP5T-2:$PC_{71}BM$ system [64]. For the first time, non-fullerene acceptor materials were synthesized into NPs in the PCE10:o-IDTBR and PBQ-QF:o-IDTBR systems, and conversion efficiencies of 5.19% and 6.52% were attained. In comparison to fullerene acceptors, o-IDTBR is the first non-fullerene acceptor to be employed in the fabrication of NPs, and like the BHJ, the conversion efficiency of OPV devices made from non-fullerene materials is higher. The maximum efficiency record among OPV devices made using NPs is 7.5%, which was achieved in the NP device fabricated by the PBQ-QF:ITIC system [53]. Of course, standard donor–acceptor materials like P3HT:$PC_{61}BM$, [56, 70], P3HT:$PC_{71}BM$ [71–73], P3HT:ICBA, and other systems are also ideal for producing NPs and OPV devices [58, 74].

4.1.2 Preparation of OPV devices from alcohol-based nanoparticles

The donor–acceptor materials utilized in alcohol-based NPs are more straightforward than those employed in water-based NPs.

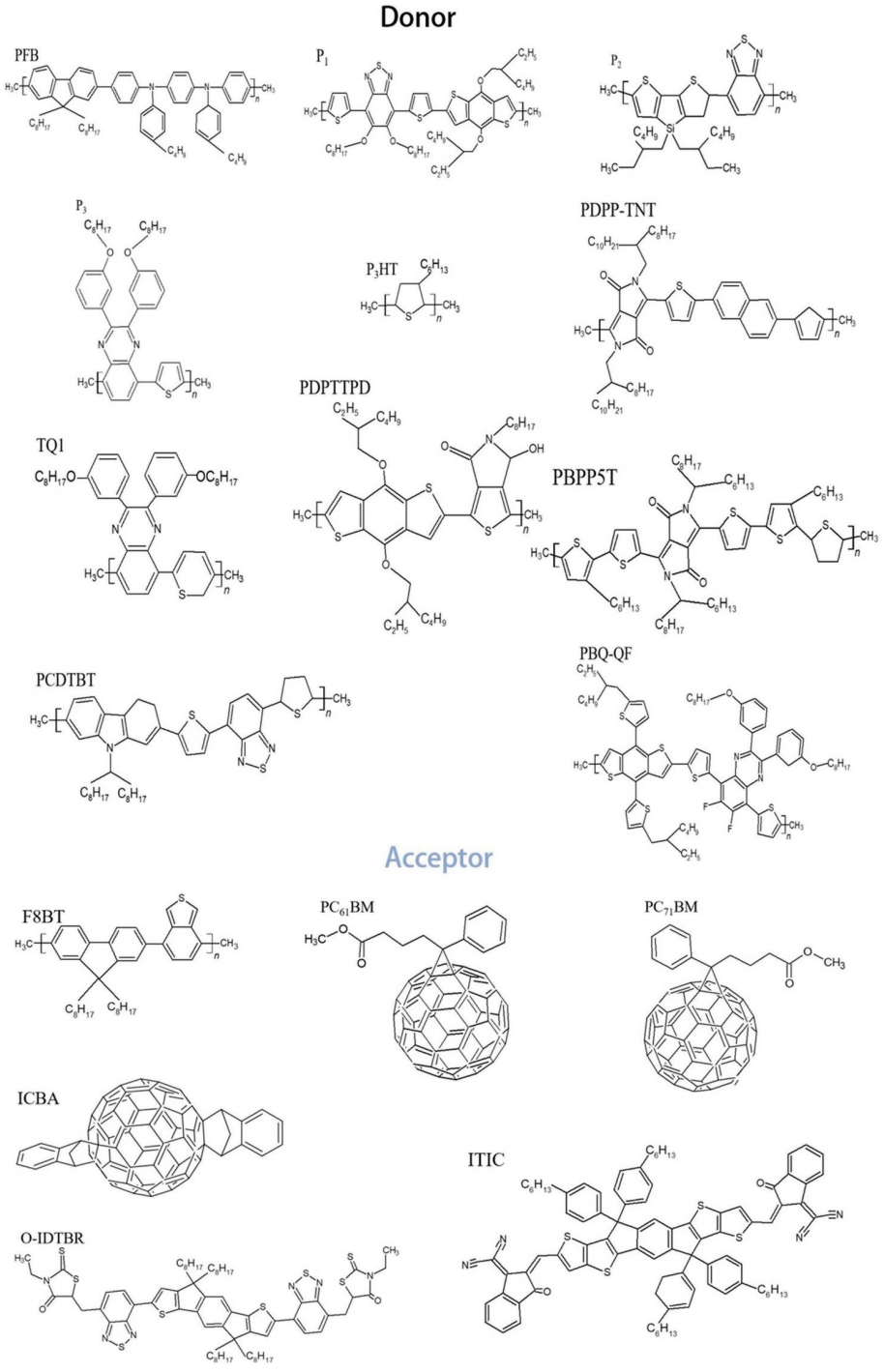

Figure 10 Molecular structures of commonly used acceptors and donors.

There are just two systems available right now, P3HT:PCBM and P3HT:ICBA. Additionally, since alcohol-based NPs are produced without the use of surfactants during the preparation process and are all produced using the nano-precipitation method. Comparing their NPs structures with those of water-based NPs produced using the miniemulsion method, the NPs produced using the nanoprecipitation method have a more uniform distribution. The alcohol-based NPs from the literatures performed better under the same circumstances [75, 76].

P3HT:PCBM NPs were fabricated by Darmawati et al. both with and without surfactants. The conversion efficiency is slightly decreased after annealing because the NPs fabricated by the miniemulsion process undergo total phase separation of the shell–core structure, resulting in distinct P3HT micro-scale domains and PCBM micro-scale domains. The donor–acceptor of NPs is not a shell–core structure in the absence of surfactants, leading to a more homogeneous mixed structure for the acceptor, which might result in more mixed and less ordered NPs [75]. By examining the distribution of P3HT:ICBA NPs in semiconductors in alcoholic dispersions of various sizes, Stefan Gärtner et al. likewise reached comparable conclusions. Small angle neutron scattering (SANS) was used to evaluate NPs with various mixing ratios, and it was shown through the use of contrast change that P3HT and ICBA were distributed uniformly throughout the NPs. The semiconductor exhibits some phase separation into tiny domains at shorter length scales, according to transient absorption spectroscopy (TAS) experiments on dispersions. TAS measurements revealed that the nanostructure and phase separation of the NPs were well retained after deposition from the dispersion and layer formation. In addition, annealing will not significantly change the nanoscale structure of the blend particles, but only integrate the NPs together to eliminate the gaps between

the nanoparticle layers, thereby enhancing the long-distance charge carrier penetration path [76]. Together, these findings explain why solar cells made from surfactant-free and precipitated NPs dispersions perform better than solar cells made using the miniemulsion technique.

Alcohol-based NPs have excellent adaptability to different coating processes. In order to fabricate an active layer, Sivaramakrishnan Sankaran et al. employed alcohol-based NPs in the spin coating, blade coating, inkjet printing, etc [77]. Then, they compared the NPs devices prepared by the above method with those prepared by dissolving in O-DCB. Among them, spin coating and blade coating were carried out in N_2 atmosphere, and devices were inverted, while ink-jet printing was carried out in air. WoO_3 NPs were added during ink-jet printing to help NPs better deposit on the hole transport layer. After annealing at 150 °C, the spin-coated active layer showed a conversion efficiency of 4.3%, which is comparable to the 5.1% of the devices made by spin-coating the O-DCB dissolved solution. The same device structure as spin coating was utilised in the blade coating process, and a cylindrical coating rod with superior control of the blade was employed to get a thickness similar to that of the spin coating, and the area was ten times larger than that of the spin coating. Finally, a conversion efficiency of 1.6% was averaged, showing that printing polymer solar cells with organic NPs dispersions is feasible. Chen et al. demonstrated a unique high-throughput robotic system that can automatically synthesize NPs of various sizes on the basis of setting up a vast area. By varying the concentration of the precursor solution and the density of the material, the particles can be manipulated precisely [78].

The device structure of OPV devices prepared with alcohol-based nanoparticles is more suitable for inverted device structure. Darmawati et al. used normal device structure at the earliest time, and then others chose the inverted device structure [79]. Stefan Gkalrtner et al. obtained 4.1% conversion efficiency of P3HT:ICBA inverted device structure prepared, which is close to 4%–6% of BHJ devices. As shown in Fig. 11, the structure diagram of the inverted device is ITO/electron transfer layer (ETL)/active layer (NPs)/hole transfer layer (HTL)/Ag (Al) from bottom to top,

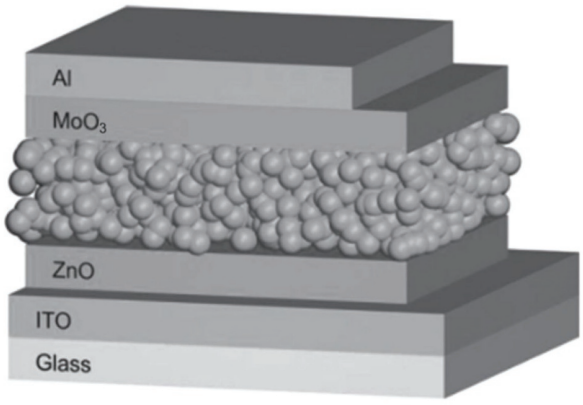

Figure 11 Schematic diagram of the inverteddevice structure. Reproduced with permission from Ref. [75], © WILEY-VCH Verlag GmbH & Co. KGaA, Weinheim 2014.

and the formal device structure is ITO/HTL/NPs/ETL/Ag (Al). The main difference lies in the spin-coating sequence of HTL and ETL. The inverted device spin-coated ELT first and then HLT, while the formal device spin-coated the reverse. Besides, alcohol solvents are also widely selected, such as methanol, ethanol, and isopropanol.

4.2 In photocatalytic hydrogen evolution

Growing interest has been shown in fabricating organic semiconductors that can power photocatalytic water splitting in recent years [80–82]. Good progress has been made in single-atom photocatalysis and Pt-based oxygen reduction reaction (ORR) nano-catalyst these years [83, 84]. The preparation of photocatalytic hydrogen evolution by organic NPs has drawn increased attention due to its low cost, excellent water stability, environmental protection, and other features, and significant progress has been accomplished [85, 86].

By using the nanoprecipitation approach to synthesize F8BT NPs, Jan Kosco et al. effectively fabricated an organic

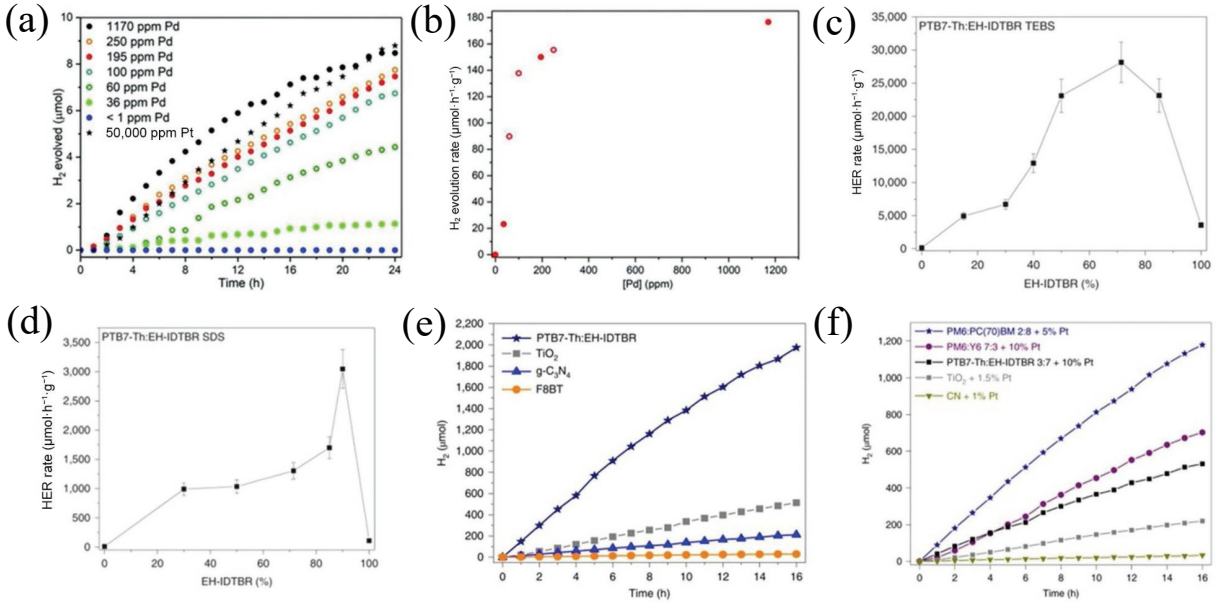

Figure 12 (a) The effect of different contents of Pt on the catalytic rate of H_2. (b) Mean H_2 release rate over 24 h as a function of Pd concentration from colloidal F8BT NPs. Reproduced with permission from Ref. [87], © WILEY-VCH Verlag GmbH & Co. KGaA, Weinheim 2018. (c) Average H_2 release rate over 16 h as a function of blend composition for PTB7-Th/EH-IDTBR NPs formed using surfactant SDS. (d) Average H_2 release rate over 16 h as a function of blend composition for PTB7-Th/EH-IDTBR NPs formed using surfactant TEBS. (e) H_2 evolution versus time for different benchmark materials. Reproduced with permission from Ref. [50], © Kosco, J. et al. 2020. (f) Average HER rate and Pt switching frequency over 16 h for optimized PM6:Y6 7:3 and PM6:PCBM 2:8 NPs compared to a series of benchmark photocatalysts. Reproduced with permission from Ref. [88], © Kosco, J. et al. 2022.

semiconductor photocatalytic hydrogen evolution system with a very minimal amount of Pd and achieved a catalytic efficiency of 8.47 mol H_2 in under 24 h, as shown in Figs. 12(a) and 12(b) [87]. After additional purification, the structure of F8BT remained unchanged while the Pd concentration in the complexes was steadily lowered to 1 ppm. Pd-NPs are evenly dispersed throughout the F8BT material. The remaining Pd is present in the NPs fabricated by processing bulk polymers, typically on the surface of the particles. The catalytic efficiency is also significantly influenced by the Pd concentration. When Pd is present in a specific concentration, the catalytic efficiency can be increased; however, when Pd is completely absent, there is no catalytic activity. Nevertheless, this technique shows that organic semiconductor nanoparticles are possible for use in photocatalytic hydrogen evolution systems. With the synthesized PTB7-Th:EH-IDTBR nanoparticles, the authors effectively constructed a hydrogen evolution system with better photocatalytic activity, as shown in Figs. 12(c) and 12(d) [50]. The size of PTB7-Th:EH-IDTBR nanoparticles and the ratio of the donor–acceptor in the particles can be changed by altering the surfactant. Under 350 to 800 nm light, the catalytic rate is more than 60,000 $mol \cdot h^{-1} \cdot g^{-1}$, the external quantum efficiency is more than 6%, and the catalytic effectiveness significantly increased. By enhancing the NPs in the PM6:Y6 and PM6:PCBM systems, Jan Kosco et al. fabricated a photocatalytic hydrogen evolution system in 2022 and achieved catalytic efficiencies of 43.9 and 73.7 $mmol \cdot h^{-1} \cdot g^{-1}$, respectively, as shown in Fig. 12(f) [88]. It was discovered that the exciton dissociates at the heterojunction of the NPs, giving charge extraction without a cocatalyst, by the characterization of transient absorption spectroscopy and photoabsorption spectroscopy. In contrast to the OPV device, the PM6:PCBM NPs of the fullerene system demonstrated better catalytic effectiveness than the non-fullerene PM6:Y6 system.

4.3 In light-emitting diodes

OLED is critical for display and has an increasingly important impact on the industry. The pollution of the solvent of OLED will greatly affect its industrial production [73, 89, 90].

Thomas Piok et al. successfully constructed OLEDs in 2003 utilising organic semiconductor polymer nanospheres after preparing m-LPPP into nanospheres with a scale of 50–500 nm by the miniemulsion process. The device, which is made of a homogeneous monolayer of nanoscale m-LPPP nanospheres, exhibits shorter onset time and somewhat greater efficiencies than conventionally produced OLEDs [57]. This phenomenon is explained by the *in-situ* production of nanostructured cathodes that resemble stalactites during the evaporation of aluminum, which improves electron injection. In 2020, Anielen H. et al. synthesized MEH-PPV:polystyrene (PS) and SY-PPV:PS NPs (the molecular structure is shown in Figs. 13(b) and 13(c)) by using the miniemulsion technology to fabricate OLEDs [91]. After multiple dialysis, the excess surfactant SDS is continuously removed, and the surface tension of the NPs dispersion system increases linearly from 38 to 60 $mN \cdot m^{-1}$, then tends to be stable, while the dispersion system maintains a certain stability. Finally, MEH-PPV:PS NPs with particle size of 65 ± 30 nm and SY-PPV:PS NPs with particle size of 125 ± 40 nm were obtained. OLEDs are finally obtained by spin coating NPs on poly(3,4-ethylenedioxythiophene):polystyrene sulfonate (PEDOT:PSS) for many times.

4.4 In organic field transistor

In recent years, new OFETs have made great achievements, and devices with higher charge carrier mobility have been fabricated [92]. The optimization of organic semiconductor materials for the preparation of OFETs requires the use of harmful organic solvents, which affect their industrial production [93].

Numerous academics have long focused on the fabrication of novel organic field effect transistors that are produced using environmentally acceptable solvents [39, 94]. P3HT NPs were fabricated in 2010 using the nanoprecipitation process by Jill E. et al. The size of the NPs was modified, and the design parameters of the semiconducting polymer NPs were initially obtained, by varying the starting P3HT concentration and the kind of poor solvent. It has been established that the initial concentration choice and the quality of the solvent have a significant impact on the size and crystallinity of NPs. Additionally, an OFET device was fabricated, having a hole mobility of around 10^{-3} $cm^2 \cdot V^{-1} \cdot s^{-1}$ [94]. In 2015, Cho et al. fabricated an OFET device with mobility of around 2.7 $cm^2 \cdot V^{-1} \cdot s^{-1}$ using a colloidal dispersion of diketopyrrolopyrrole-thienothiophene (DPP-TT) in butyl acetate and ethyl acetate [95]. In 2016, Cho fabricated DPP-TT water-based NPs dispersion system using miniemulsion technology. When annealed at 200 °C, due to the influence of surfactant SDS, the mobility of the constructed OFET device is only about 0.0005 $cm^2 \cdot V^{-1} \cdot s^{-1}$. With the increase of annealing temperature, when the temperature reaches 270 °C, the active layer undergoes a second phase transition, effectively removing SDS and obtaining a mobility of about 0.3 $cm^2 \cdot V^{-1} \cdot s^{-1}$, almost the same as that of the chlorobenzene-based device [96]. Figures 14(d) and 14(e) show the AFM images of PBTTT NPs films after thermal annealing at 200 and 270 °C, respectively.

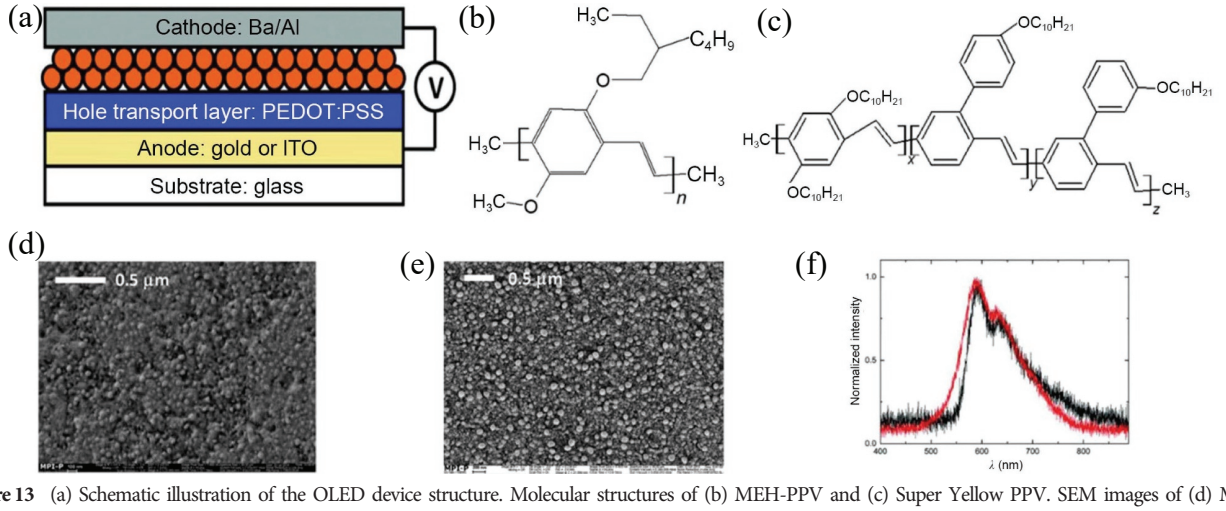

Figure 13 (a) Schematic illustration of the OLED device structure. Molecular structures of (b) MEH-PPV and (c) Super Yellow PPV. SEM images of (d) MEH-PPV:PS and (e) SY-PPV:PS NPs films. (f) Electroluminescence emission spectra of a MEH-PPV:PS nanoparticle-based PLED (red) and a reference device based on a solution-based MEH-PPV:PS hybrid. Reproduced with permission from Ref. [91], © The Royal Society of Chemistry 2020.

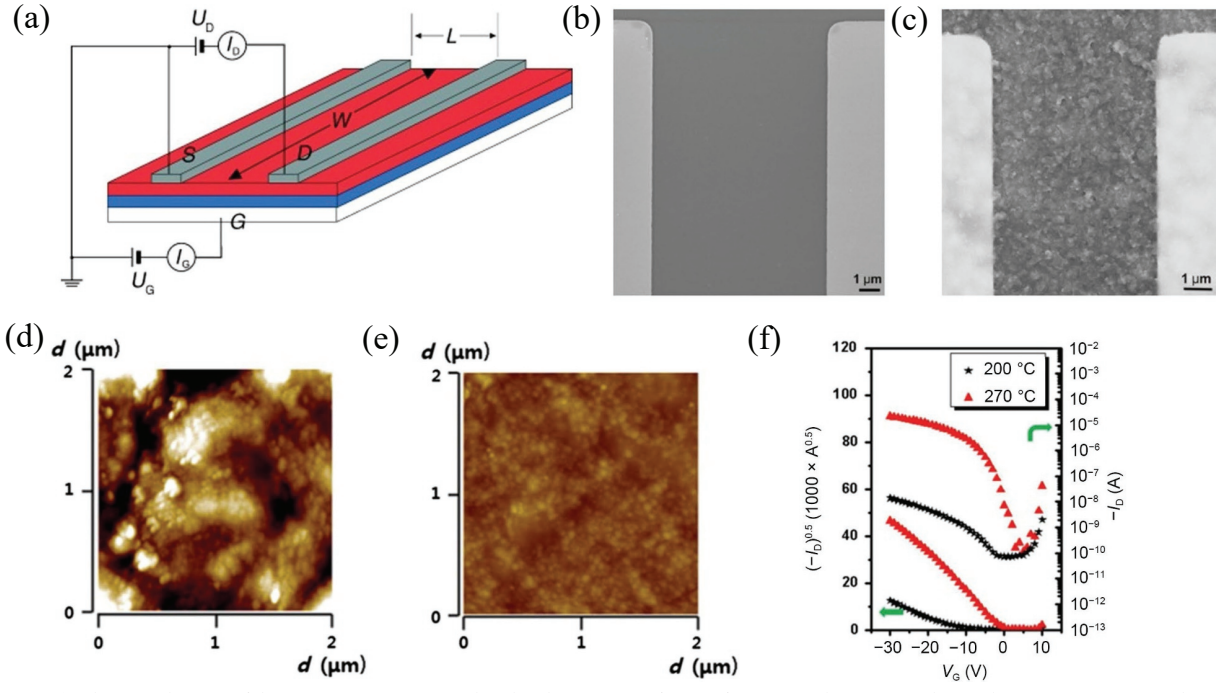

Figure 14 (a) Schematic diagram of the OFET structure. Reproduced with permission from Ref. [97], © Wiley-VCH Verlag GmbH & Co. KGaA, Weinheim 2008. (b) SEM image of OFET fabricated by P3HT NPs. (c) SEM image of OFET prepared by P3HT dissolved in chloroform. Reproduced with permission from Ref. [94], © American Chemical Society 2010. AFM images of PBTTT NPs films after thermal annealing at (d) 200 °C and (e) 270 °C. (f) Transfer characteristics of nanoparticle-based PFETs annealed at 200 and 270 °C. Reproduced with permission from Ref. [96], © Elsevier B.V. 2015.

Table 1 Reported evolution of the efficiency of OPV devices fabricated from aqueous nanoparticles

Year	Materials	J_{sc} (mA·cm^{-2})	V_{oc} (V)	FF (%)	PCE (%)	Ref.
2003	F8BT:PFB	—	—	—	0.004	[55]
2011	PSBTBT:PCBM	3.99	0.47	29.3	0.55	[66]
2012	F8BT:PFB	1.81	0.77	28.0	0.39	[52]
2013	P3HT:ICBA	5.57	0.79	57.0	2.50	[58]
2014	P3HT:PCBM	6.38	0.51	66.2	2.15	[71]
2015	P(TBT-DPP):ICBA	12.73	0.44	47.0	2.63	[68]
2016	TQ1:PC71BM	10.06	0.70	36.0	2.54	[60]
2017	PBDTTPD:PC71BM	9.99	0.86	44.0	3.80	[61]
2018	PBQ-QF:ITIC	15.17	0.87	55.6	7.50	[53]
2019	P3HT:ICXA	4.40	0.58	59.1	1.20	[74]
2021	PCBM:BCP	10.61	0.64	36.7	2.54	[98]

Table 2 Reported evolution table of OPV device efficiencies prepared from alcohol-based nanoparticles

Year	Materials	J_{sc} (mA·cm^{-2})	V_{oc} (V)	FF (%)	PCE (%)	Ref.
2014	P3HT:PCBM	4.84	0.63	36.0	1.09	[79]
2015	P3HT:ICBA	9.00	0.78	58.0	4.10	[75]
2016	P3HT:ICBA	9.40	0.83	55.0	4.30	[77]
2017	P3HT:ICBA	9.20	0.80	53.0	3.90	[76]
2018	P3HT:ICBA	9.74	0.81	56.5	4.52	[78]

5 Conclusions

In this review, we summarize the application of organic nanoparticles in semiconductor devices over the last 20 years from preparation techniques to active layer formation in colloidal dispersions. Obviously, after many years of development, it has been used in some applications, especially in OPV, where NP devices with an efficiency of 7.5% have been successfully obtained. Some progress has also been made in photocatalysis and organic light-emitting diodes.

Miniemulsion and nanoprecipitation are the two main techniques used to prepare nanoparticle dispersions. Both are discussed in depth, especially the experimental parameters that affect the size of nanoparticles. The morphology inside the NPs is also interesting because the distribution of donor and acceptor domains drives charge generation and charge transport efficiency. The morphology inside the NPs varies depending on the technique used, and NPs prepared by miniemulsion have been reported to exhibit shell–core morphology, while NPs prepared by nanoprecipitation have no obvious shell–core distribution.

Organic NPs will undoubtedly play a larger role in semiconductors in the future. At the same time, it faces some difficulties. For example, OPV efficiency is insufficient, and the performance of hydrogen catalysis and traditional light-emitting diodes falls short of that of traditional semiconductor devices. Here are some possibilities:

(1) Currently, most efficient polymeric semiconductors have complicated molecular structures, making it difficult to prepare nanoparticles suitable for organic semiconductor preparation. Simple small molecule materials to prepare nanoparticles will be a possible strategy for future development.

(2) Surfactant is inseparable from the preparation process, but it has an effect on semiconductor performance. It is a good strategy to look for a surface activity that has little impact on semiconductor performance and to improve surfactant removal.

(3) The distribution of donor and acceptor in NPs is not as uniform as that in solution, so the morphology, donor, and acceptor distribution of the prepared active layer film are not optimal. It is a good direction to find ways to improve the film morphology.

There is still a long way to go for the widespread application of NPs in semiconductors, but there is bound to be a bright future.

Acknowledgements

This work was financially supported by the National Natural Science Foundation of China (Nos. 21922505 and 52273245) and the Strategic Priority Research Program of Chinese Academy of Sciences (No. XDB36000000).

References

[1] Ferraris, J.; Cowan, D. O.; Walatka, V.; Perlstein, J. H. Electron transfer in a new highly conducting donor–acceptor complex. *J. Am. Chem. Soc.* **1973**, *95*, 948–949.

[2] Shirakawa, H.; Louis, E. J.; MaCdiarmid, A. G.; Ching, C. K.; Heeger, A. J. Synthesis of electrically conducting organic polymers: Halogen derivatives of polyacetylene, $(CH)_x$. *J. Chem. Soc. Chem. Commun.* **1977**, 578–580.

[3] Granström, M.; Petritsch, K.; Arias, A. C.; Lux, A.; Andersson, M. R.; Friend, R. H. Laminated fabrication of polymeric photovoltaic diodes. *Nature* **1998**, *395*, 257–260.

[4] Li, X. J.; Pan, F.; Sun, C. K.; Zhang, M.; Wang, Z. W.; Du, J. Q.; Wang, J.; Xiao, M.; Xue, L. W.; Zhang, Z. G. et al. Simplified synthetic routes for low cost and high photovoltaic performance n-type organic semiconductor acceptors. *Nat. Commun.* **2019**, *10*, 519.

[5] Chen, Y. N.; Zhao, Y.; Liang, Z. Q. Solution processed organic thermoelectrics: Towards flexible thermoelectric modules. *Energy Environ. Sci.* **2015**, *8*, 401–422.

[6] Qian, Y.; Zhang, X. W.; Qi, D. P.; Xie, L. H.; Chandran, B. K.; Chen, X. D.; Huang, W. Thin-film organic semiconductor devices: From flexibility to ultraflexibility. *Sci. China Mater.* **2016**, *59*, 589–608.

[7] Qian, Y.; Zhang, X. W.; Xie, L. H.; Qi, D. P.; Chandran, B. K.; Chen, X. D.; Huang, W. Stretchable organic semiconductor devices. *Adv. Mater.* **2016**, *28*, 9243–9265.

[8] Kubo, T.; Häusermann, R.; Tsurumi, J.; Soeda, J.; Okada, Y.; Yamashita, Y.; Akamatsu, N.; Shishido, A.; Mitsui, C.; Okamoto, T. et al. Suppressing molecular vibrations in organic semiconductors by inducing strain. *Nat. Commun.* **2016**, *7*, 11156.

[9] Stolle, A.; Szuppa, T.; Leonhardt, S. E. S.; Ondruschka, B. Ball milling in organic synthesis: Solutions and challenges. *Chem. Soc. Rev.* **2011**, *40*, 2317–2329.

[10] Wang, G. W. Mechanochemical organic synthesis. *Chem. Soc. Rev.* **2013**, *42*, 7668–7700.

[11] Báti, G.; Csókás, D.; Yong, T.; Tam, S. M.; Shi, R. R. S.; Webster, R. D.; Pápai, I.; García, F.; Stuparu, M. C. Mechanochemical synthesis of corannulene-based curved nanographenes. *Angew. Chem., Int. Ed.* **2020**, *59*, 21620–21626.

[12] Seo, T.; Toyoshima, N.; Kubota, K.; Ito, H. Tackling solubility issues in organic synthesis: Solid-state cross-coupling of insoluble aryl halides. *J. Am. Chem. Soc.* **2021**, *143*, 6165–6175.

[13] Qin, Z. S.; Gao, C.; Gao, H. K.; Wang, T. Y.; Dong, H. L.; Hu, W. P. Molecular doped, color-tunable, high-mobility, emissive, organic semiconductors for light-emitting transistors. *Sci. Adv.* **2022**, *8*, eabp8775.

[14] Giri, G.; Verploegen, E.; Mannsfeld, S. C. B.; Atahan-Evrenk, S.; Kim, D. H.; Lee, S. Y.; Becerril, H. A.; Aspuru-Guzik, A.; Toney, M. F.; Bao, Z. N. Tuning charge transport in solution-sheared organic semiconductors using lattice strain. *Nature* **2011**, *480*, 504–508.

[15] Gao, P.; Beckmann, D.; Tsao, H. N.; Feng, X. L.; Enkelmann, V.; Baumgarten, M.; Pisula, W.; Müllen, K. Dithieno[2,3-d;2',3'-d ′]benzo[1,2-b;4,5-b']dithiophene (DTBDT) as semiconductor for high-performance, solution-processed organic field-effect transistors. *Adv. Mater.* **2009**, *21*, 213–216.

[16] Ho, D.; Lee, J.; Park, S.; Park, Y.; Cho, K.; Campana, F.; Lanari, D.; Facchetti, A.; Seo, S.; Kim, C. et al. Green solvents for organic thin-film transistor processing. *J. Mater. Chem. C* **2020**, *8*, 5786–5794.

[17] Walker, B.; Tamayo, A.; Duong, D. T.; Dang, X. D.; Kim, C.; Granstrom, J.; Nguyen, T. Q. A systematic approach to solvent selection based on cohesive energy densities in a molecular bulk heterojunction system. *Adv. Energy Mater.* **2011**, *1*, 221–229.

[18] Campana, F.; Lanari, D.; Marrocchi, A.; Vaccaro, L. Green solvents for organic electronics processing. In *Sustainable Strategies in Organic Electronics*; Marrocchi, A., Ed; Elsevier: Amsterdam, 2022; pp 425–462.

[19] Henderson, R. K.; Jiménez-González, C.; Constable, D. J. C.; Alston, S. R.; Inglis, G. G. A.; Fisher, G.; Sherwood, J.; Binks, S. P.; Curzons, A. D. Expanding GSK's solvent selection guide-embedding sustainability into solvent selection starting at medicinal chemistry. *Green Chem.* **2011**, *13*, 854–862.

[20] Li, S. L.; Zhang, H.; Yue, S. L.; Yu, X.; Zhou, H. Q. Recent advances in non-fullerene organic photovoltaics enabled by green solvent processing. *Nanotechnology* **2022**, *33*, 072002.

[21] Duan, C. H.; Zhang, K.; Zhong, C. M.; Huang, F.; Cao, Y. Recent advances in water/alcohol-soluble π-conjugated materials: New materials and growing applications in solar cells. *Chem. Soc. Rev.* **2013**, *42*, 9071–9104.

[22] Tada, K. Yet another poor man's green bulk heterojunction photocells: Annealing effect and film composition dependence of photovoltaic devices using poly(3-hexylthiophene): C_{70} composites prepared with chlorine-free solvent. *Sol. Energy Mater. Sol. Cells* **2013**, *108*, 82–86.

[23] Campana, F.; Kim, C.; Marrocchi, A.; Vaccaro, L. Green solvent-processed organic electronic devices. *J. Mater. Chem. C* **2020**, *8*, 15027–15047.

[24] Lee, W. Y.; Giri, G.; Diao, Y.; Tassone, C. J.; Matthews, J. R.; Sorensen, M. L.; Mannsfeld, S. C. B.; Chen, W. C.; Fong, H. H.; Tok, J. B. H. et al. Effect of non-chlorinated mixed solvents on charge transport and morphology of solution-processed polymer field-effect transistors. *Adv. Funct. Mater.* **2014**, *24*, 3524–3534.

[25] Zhang, L. Z.; Zhou, X. Y.; Zhong, X. W.; Cheng, C.; Tian, Y. Q.; Xu, B. M. Hole-transporting layer based on a conjugated polyelectrolyte with organic cations enables efficient inverted perovskite solar cells. *Nano Energy* **2019**, *57*, 248–255.

[26] Chen, Y.; Zhang, S. Q.; Wu, Y.; Hou, J. H. Molecular design and morphology control towards efficient polymer solar cells processed using non-aromatic and non-chlorinated solvents. *Adv. Mater.* **2014**, *26*, 2744–2749.

[27] Zhao, Y.; Xie, Z. Y.; Qin, C. J.; Qu, Y.; Geng, Y. H.; Wang, L. X. Enhanced charge collection in polymer photovoltaic cells by using an ethanol-soluble conjugated polyfluorene as cathode buffer layer. *Sol. Energy Mater. Sol. Cells* **2009**, *93*, 604–608.

[28] Yassar, A.; Miozzo, L.; Gironda, R.; Horowitz, G. Rod-coil and all-conjugated block copolymers for photovoltaic applications. *Prog. Polym. Sci.* **2013**, *38*, 791–844.

[29] Tang, F.; Wu, K. L.; Zhou, Z. J.; Wang, G.; Zhao, B.; Tan, S. T.

Alkynyl-functionalized pyrene-cored perylene diimide electron acceptors for efficient nonfullerene organic solar cells. *ACS Appl. Energy Mater.* **2019**, *2*, 3918–3926.
[30] Ding, S.; Ni, Z. J.; Hu, M. X.; Qiu, G. G.; Li, J.; Ye, J.; Zhang, X. T.; Liu, F.; Dong, H. L.; Hu, W. P. An asymmetric furan/thieno[3, 2-b]thiophene diketopyrrolopyrrole building block for annealing-free green-solvent processable organic thin-film transistors. *Macromol. Rapid Commun.* **2018**, *39*, 1800225.
[31] Choi, H. H.; Baek, J. Y.; Song, E.; Kang, B.; Cho, K.; Kwon, S. K.; Kim, Y. H. A pseudo-regular alternating conjugated copolymer using an asymmetric monomer: A high-mobility organic transistor in nonchlorinated solvents. *Adv. Mater.* **2015**, *27*, 3626–3631.
[32] Li, Z. Y.; Ying, L.; Zhu, P.; Zhong, W. K.; Li, N.; Liu, F.; Huang, F.; Cao, Y. A generic green solvent concept boosting the power conversion efficiency of all-polymer solar cells to 11%. *Energy Environ. Sci.* **2019**, *12*, 157–163.
[33] Zhao, W. C.; Zhang, S. Q.; Zhang, Y.; Li, S. S.; Liu, X. Y.; He, C.; Zheng, Z.; Hou, J. H. Environmentally friendly solvent-processed organic solar cells that are highly efficient and adaptable for the blade-coating method. *Adv. Mater.* **2018**, *30*, 1704837.
[34] Ma, Z. W.; Zhao, B.; Gong, Y. S.; Deng, J. P.; Tan, Z. A. Green-solvent-processable strategies for achieving large-scale manufacture of organic photovoltaics. *J. Mater. Chem. A* **2019**, *7*, 22826–22847.
[35] Rao, J. P.; Geckeler, K. E. Polymer nanoparticles: Preparation techniques and size-control parameters. *Prog. Polym. Sci.* **2011**, *36*, 887–913.
[36] Li, K. X.; Zhang, T. L.; Li, H. Z.; Li, M. Z., Song, Y. L. The precise assembly of nanoparticles. *Acta Phys. Chim. Sin.* **2020**, *36*, 1911057.
[37] Mishchuk, N. A.; Verbich, S. V.; Dukhin, S. S.; Holt, Ø.; Sjöblom, J. Rapid brownian coagulation in dilute polydisperse emulsions. *J. Dispersion Sci. Technol.* **1997**, *18*, 517–537.
[38] Kabalnov, A. S.; Pertzov, A. V.; Shchukin, E. D. Ostwald ripening in emulsions: I. Direct observations of Ostwald ripening in emulsions. *J. Colloid Interface Sci.* **1987**, *118*, 590–570.
[39] Landfester, K.; Montenegro, R.; Scherf, U.; Güntner, R.; Asawapirom, U.; Patil, S.; Neher, D.; Kietzke, T. Semiconducting polymer nanospheres in aqueous dispersion prepared by a miniemulsion process. *Adv. Mater.* **2002**, *14*, 651–655.
[40] Fessi, H.; Puisieux, F.; Devissaguet, J. P.; Ammoury, N.; Benita, S. Nanocapsule formation by interfacial polymer deposition following solvent displacement. *Int. J. Pharm.* **1989**, *55*, R1–R4.
[41] Mora-Huertas, C. E.; Fessi, H.; Elaissari, A. Influence of process and formulation parameters on the formation of submicron particles by solvent displacement and emulsification-diffusion methods: Critical comparison. *Adv. Colloid Interface Sci.* **2011**, *163*, 90–122.
[42] Gavory, C.; Durand, A.; Six, J. L.; Nouvel, C.; Marie, E.; Leonard, M. Polysaccharide-covered nanoparticles prepared by nanoprecipitation. *Carbohydr. Polym.* **2011**, *84*, 133–140.
[43] Holmes. A.; Deniau, E.; Lartigau-Dagron, C.; Bousquet, A.; Chambon, S.; Holmes, N. P. Review of waterborne organicsemiconductor colloids for photovoltaics. *ACS Nano* **2021**, *15*, 3927–3959.
[44] Landfester, K. The generation of nanoparticles in miniemulsions. *Adv. Mater.* **2001**, *13*, 765–768.
[45] Aubry, J.; Ganachaud, F.; Addad, J. P. C.; Cabane, B. Nanoprecipitation of polymethylmethacrylate by solvent shifting: 1. Boundaries. *Langmuir* **2009**, *25*, 1970–1979.
[46] Chambon, S.; Schatz, C.; Sébire, V.; Pavageau, B.; Wantz, G.; Hirsch, L. Organic semiconductor core–shell nanoparticles designed through successive solvent displacements. *Mater. Horiz.* **2014**, *1*, 431–438.
[47] Palacio Valera, A.; Schatz, C.; Ibarboure, E.; Kubo, T.; Segawa, H.; Chambon, S. Elaboration of PCBM coated P3HT nanoparticles: Understanding the shell formation. *Front. Energy Res.* **2019**, *6*, 146.
[48] Tan, B.; Li, Y. C.; Palacios, M. F.; Therrien, J.; Sobkowicz, M. J. Effect of surfactant conjugation on structure and properties of poly(3-hexylthiophene) colloids and field effect transistors. *Colloids Surf. A: Physicochem. Eng. Aspects* **2016**, *488*, 7–14.
[49] Cho, J.; Yoon, S.; Sim, K. M.; Jeong, Y. J.; Park, C. E.; Kwon, S. K.; Kim, Y. H.; Chung, D. S. Universal selection rule for surfactants used in miniemulsion processes for eco-friendly and high performance polymer semiconductors. *Energy Environ. Sci.* **2017**, *10*, 2324–2333.
[50] Kosco, J.; Bidwell, M.; Cha, H.; Martin, T.; Howells, C. T.; Sachs, M.; Anjum, D. H.; Lopez, S. G.; Zou, L. Y.; Wadsworth, A. et al. Enhanced photocatalytic hydrogen evolution from organic semiconductor heterojunction nanoparticles. *Nat. Mater.* **2020**, *19*, 559–565.
[51] Cho, J.; Cheon, K. H.; Ahn, H.; Park, K. H.; Kwon, S. K.; Kim, Y. H.; Chung, D. S. High charge-carrier mobility of 2.5 $cm^2 \cdot V^{-1} \cdot s^{-1}$ from a water-borne colloid of a polymeric semiconductor via smart surfactant engineering. *Adv. Mater.* **2015**, *27*, 5587–5592.
[52] Stapleton, A.; Vaughan, B.; Xue, B. F.; Sesa, E.; Burke, K.; Zhou, X. J.; Bryant, G.; Werzer, O.; Nelson, A.; Kilcoyne, A. L. D. et al. A multilayered approach to polyfluorene water-based organic photovoltaics. *Sol. Energy Mater. Sol. Cells* **2012**, *102*, 114–124.
[53] Xie, C.; Heumüller, T.; Gruber, W.; Tang, X. F.; Classen, A.; Schuldes, I.; Bidwell, M.; Späth, A.; Fink, R. H.; Unruh, T. et al. Overcoming efficiency and stability limits in water-processing nanoparticular organic photovoltaics by minimizing microstructure defects. *Nat. Commun.* **2018**, *9*, 5335.
[54] Colberts, F. J. M.; Wienk, M. M.; Janssen, R. A. J. Aqueous nanoparticle polymer solar cells: Effects of surfactant concentration and processing on device performance. *ACS Appl. Mater. Interfaces* **2017**, *9*, 13380–13389.
[55] Kietzke, T.; Neher, D.; Landfester, K.; Montenegro, R.; Güntner, R.; Scherf, U. Novel approaches to polymer blends based on polymer nanoparticles. *Nat. Mater.* **2003**, *2*, 408–412.
[56] Ulum, S.; Holmes, N.; Darwis, D.; Burke, K.; Kilcoyne, A. L. D.; Zhou, X. J.; Belcher, W.; Dastoor, P. Determining the structural motif of P3HT: PCBM nanoparticulate organic photovoltaic devices. *Sol. Energy Mater. Sol. Cells* **2013**, *110*, 43–48.
[57] Piok, T.; Gamerith, S.; Gadermaier, C.; Plank, H.; Wenzl, F. P.; Patil, S.; Montenegro, R.; Kietzke, T.; Neher, D.; Scherf, U. et al. Organic light-emitting devices fabricated from semiconducting nanospheres. *Adv. Mater.* **2003**, *15*, 800–804.
[58] Ulum, S.; Holmes, N.; Barr, M.; Kilcoyne, A. L. D.; Gong, B. B.; Zhou, X. J.; Belcher, W.; Dastoor, P. The role of miscibility in polymer: Fullerene nanoparticulate organic photovoltaic devices. *Nano Energy* **2013**, *2*, 897–905.
[59] Holmes, N. P.; Nicolaidis, N.; Feron, K.; Barr, M.; Burke, K. B.; Al-Mudhaffer, M.; Sista, P.; Kilcoyne, A. L. D.; Stefan, M. C.; Zhou, X. J. et al. Probing the origin of photocurrent in nanoparticulate organic photovoltaics. *Sol. Energy Mater. Sol. Cells* **2015**, *140*, 412–421.
[60] Holmes, N. P.; Marks, M.; Kumar, P.; Kroon, R.; Barr, M. G.; Nicolaidis, N.; Feron, K.; Pivrikas, A.; Fahy, A.; de Zerio Mendaza, A. D. et al. Nano-pathways: Bridging the divide between water-processable nanoparticulate and bulk heterojunction organic photovoltaics. *Nano Energy* **2016**, *19*, 495–510.
[61] D'Olieslaeger, L.; Pirotte, G.; Cardinaletti, I.; D'Haen, J.; Manca, J.; Vanderzande, D.; Maes, W.; Ethirajan, A. Eco-friendly fabrication of PBDTTPD:PC_{71}BM solar cells reaching a PCE of 3.8% using water-based nanoparticle dispersions. *Org. Electron.* **2017**, *42*, 42–46.
[62] Prunet, G.; Parrenin, L.; Pavlopoulou, E.; Pecastaings, G.; Brochon, C.; Hadziioannou, G.; Cloutet, E. Aqueous PCDTBT:PC_{71}BM photovoltaic inks made by nanoprecipitation. *Macromol. Rapid Commun.* **2018**, *39*, 1700504.
[63] Parrenin, L.; Laurans, G.; Pavlopoulou, E.; Fleury, G.; Pecastaings, G.; Brochon, C.; Vignau, L.; Hadziioannou, G.; Cloutet, E. Photoactive donor–acceptor composite nanoparticles dispersed in water. *Langmuir* **2017**, *33*, 1507–1515.
[64] Xie, C.; Classen, A.; Späth, A.; Tang, X. F.; Min, J.; Meyer, M.; Zhang, C. H.; Li, N.; Osvet, A.; Fink, R. H. et al. Overcoming microstructural limitations in water processed organic solar cells by engineering customized nanoparticulate inks. *Adv. Energy Mater.* **2018**, *8*, 1702857.
[65] Pan, X.; Sharma, A.; Gedefaw, D.; Kroon, R.; de Zerio, A. D.; Holmes, N. P.; Kilcoyne, A. L. D.; Barr, M. G.; Fahy, A.; Marks, M. et al. Environmentally friendly preparation of nanoparticles for

organic photovoltaics. *Org. Electron.* **2018**, *59*, 432–440.
[66] Andersen, T. R.; Larsen-Olsen, T. T.; Andreasen, B.; Böttiger, A. P. L.; Carlé, J. E.; Helgesen, M.; Bundgaard, E.; Norrman, K.; Andreasen, J. W.; Jørgensen, M.; Krebs, F. C. Aqueous processing of low-band-gap polymer solar cells using roll-to-roll methods. *ACS Nano* **2011**, *5*, 4188–4196.
[67] Vaughan, B.; Williams, E. L.; Holmes, N. P.; Sonar, P.; Dodabalapur, A.; Dastoor, P. C.; Belcher, W. J. Water-based nanoparticulate solar cells using a diketopyrrolopyrrole donor polymer. *Phys. Chem. Chem. Phys.* **2014**, *16*, 2647–2653.
[68] Yamamoto, N. A. D.; Payne, M. E.; Koehler, M.; Facchetti, A.; Roman, L. S.; Arias, A. C. Charge transport model for photovoltaic devices based on printed polymer: Fullerene nanoparticles. *Sol. Energy Mater. Sol. Cells* **2015**, *141*, 171–177.
[69] D'Olieslaeger, L.; Pfannmöller, M.; Fron, E.; Cardinaletti, I.; Van Der Auweraer, M.; Van Tendeloo, G.; Bals, S.; Maes, W.; Vanderzande, D.; Manca, J. et al. Tuning of PCDTBT:$PC_{71}BM$ blend nanoparticles for eco-friendly processing of polymer solar cells. *Sol. Energy Mater. Sol. Cells* **2017**, *159*, 179–188.
[70] Larsen-Olsen, T. T.; Andreasen, B.; Andersen, T. R.; Böttiger, A. P. L.; Bundgaard, E.; Norrman, K.; Andreasen, J. W.; Jørgensen, M.; Krebs, F. C. Simultaneous multilayer formation of the polymer solar cell stack using roll-to-roll double slot-die coating from water. *Sol. Energy Mater. Sol. Cells* **2012**, *97*, 22–27.
[71] Gehan, T. S.; Bag, M.; Renna, L. A.; Shen, X. B.; Algaier, D. D.; Lahti, P. M.; Russell, T. P.; Venkataraman, D. Multiscale active layer morphologies for organic photovoltaics through self-assembly of nanospheres. *Nano Lett.* **2014**, *14*, 5238–5243.
[72] Holmes, N. P.; Ulum, S.; Sista, P.; Burke, K. B.; Wilson, M. G.; Stefan, M. C.; Zhou, X. J.; Dastoor, P. C.; Belcher, W. J. The effect of polymer molecular weight on P3HT:PCBM nanoparticulate organic photovoltaic device performance. *Sol. Energy Mater. Sol. Cells* **2014**, *128*, 369–377.
[73] Bag, M.; Gehan, T. S.; Renna, L. A.; Algaier, D. D.; Lahti, P. M.; Venkataraman, D. Fabrication conditions for efficient organic photovoltaic cells from aqueous dispersions of nanoparticles. *RSC Adv.* **2014**, *4*, 45325–45331.
[74] Almyahi, F.; Andersen, T. R.; Fahy, A.; Dickinson, M.; Feron, K.; Belcher, W. J.; Dastoor, P. C. The role of surface energy control in organic photovoltaics based on solar paints. *J. Mater. Chem. A* **2019**, *7*, 9202–9214.
[75] Gärtner, S.; Christmann, M.; Sankaran, S.; Röhm, H.; Prinz, E. M.; Penth, F.; Pütz, A.; Türeli, A. E.; Penth, B.; Baumstümmler, B. et al. Eco-friendly fabrication of 4% efficient organic solar cells from surfactant-free P3HT:ICBA nanoparticle dispersions. *Adv. Mater.* **2014**, *26*, 6653–6657.
[76] Gärtner, S.; Clulow, A. J.; Howard, I. A.; Gilbert, E. P.; Burn, P. L.; Gentle, I. R.; Colsmann, A. Relating structure to efficiency in surfactant-free polymer/fullerene nanoparticle-based organic solar cells. *ACS Appl. Mater. Interfaces* **2017**, *9*, 42986–42995.
[77] Sankaran, S.; Glaser, K.; Gärtner, S.; Rödlmeier, T.; Sudau, K.; Hernandez-Sosa, G.; Colsmann, A. Fabrication of polymer solar cells from organic nanoparticle dispersions by doctor blading or ink-jet printing. *Org. Electron.* **2016**, *28*, 118–122.
[78] Xie, C.; Tang, X. F.; Berlinghof, M.; Langner, S.; Chen, S.; Späth, A.; Li, N.; Fink, R. H.; Unruh, T.; Brabec, C. J. Robot-based high-throughput engineering of alcoholic polymer: Fullerene nanoparticle inks for an eco-friendly processing of organic solar cells. *ACS Appl. Mater. Interfaces* **2018**, *10*, 23225–23234.
[79] Darwis, D.; Holmes, N.; Elkington, D.; David Kilcoyne, A. L.; Bryant, G.; Zhou, X. J.; Dastoor, P.; Belcher, W. Surfactant-free nanoparticulate organic photovoltaics. *Sol. Energy Mater. Sol. Cells* **2014**, *121*, 99–107.
[80] Wolff, C. M.; Frischmann, P. D.; Schulze, M.; Bohn, B. J.; Wein, R.; Livadas, P.; Carlson, M. T.; Jäckel, F.; Feldmann, J.; Würthner, F. et al. All-in-one visible-light-driven water splitting by combining nanoparticulate and molecular co-catalysts on CdS nanorods. *Nat. Energy* **2018**, *3*, 862–869.
[81] Tahir, M.; Tasleem, S.; Tahir, B. Recent development in band engineering of binary semiconductor materials for solar driven photocatalytic hydrogen production. *Int. J. Hydrogen Energy* **2020**, *45*, 15985–16038.
[82] Pan, J. B.; Shen, S.; Zhou, W.; Tang, J.; Ding, H. Z.; Wang, J. B.; Chen, L.; Au, C. T.; Yin, S. F. Recent progress in photocatalytic hydrogen evolution. *cta Phys.—Chim. Sin.* **2020**, *36*, 1905068.
[83] Wang, Y.; Wang, D. S.; Li, Y. D. A fundamental comprehension and recent progress in advanced Pt-based ORR nanocatalysts. *SmartMat* **2021**, *2*, 56–75.
[84] Zhang, D. P.; Li, Y. X.; Li, Y.; Zhan, S. H. Towards single-atom photocatalysts for future carbon-neutral application. *SmartMat* **2022**, *3*, 417–446.
[85] Liu, A. J.; Tai, C. W.; Holá, K.; Tian, H. N. Hollow polymer dots: Nature-mimicking architecture for efficient photocatalytic hydrogen evolution reaction. *J. Mater. Chem. A* **2019**, *7*, 4797–4803.
[86] Wang, L.; Fernández-Terán, R.; Zhang, L.; Fernandes, D. L. A.; Tian, L.; Chen, H.; Tian, H. N. Organic polymer dots as photocatalysts for visible light-driven hydrogen generation. *Angew. Chem., Int. Ed.* **2016**, *55*, 12306–12310.
[87] Kosco, J.; Sachs, M.; Godin, R.; Kirkus, M.; Francas, L.; Bidwell, M.; Qureshi, M.; Anjum, D.; Durrant, J. R.; McCulloch, I. The effect of residual palladium catalyst contamination on the photocatalytic hydrogen evolution activity of conjugated polymers. *Adv. Energy Mater.* **2018**, *8*, 1802181.
[88] Kosco, J.; Gonzalez-Carrero, S.; Howells, C. T.; Fei, T.; Dong, Y. F.; Sougrat, R.; Harrison, G. T.; Firdaus, Y.; Sheelamanthula, R.; Purushothaman, B. et al. Generation of long-lived charges in organic semiconductor heterojunction nanoparticles for efficient photocatalytic hydrogen evolution. *Nat. Energy* **2022**, *7*, 340–351.
[89] Zhou, K.; Tang, J.; Fang, S. F.; Jiang, K.; Yang, F. X.; Ji, D. Y.; Xiang, J.; Liu, J.; Dong, H. L.; Han, C. et al. Efficient energy transfer in organic light-emitting transistor with tunable wavelength. *Nano Res.* **2021**, *15*, 3647–3652.
[90] Zheng, L.; Li, J. F.; Zhou, K.; Yu, X. X.; Zhang, X. T.; Dong, H. L.; Hu, W. P. Molecular-scale integrated multi-functions for organic light-emitting transistors. *Nano Res.* **2020**, *13*, 1976–1981.
[91] Ribeiro, A. H.; Fakih, A.; van der Zee, B.; Veith, L.; Glaser, G.; Kunz, A.; Landfester, K.; Blom, P. W. M.; Michels, J. J. Green and stable processing of organic light-emitting diodes from aqueous nanodispersions. *J. Mater. Chem. C* **2020**, *8*, 6528–6535.
[92] Kim, G.; Kang, S. J.; Dutta, G. K.; Han, Y. K.; Shin, T. J.; Noh, Y. Y.; Yang, C. A thienoisoindigo-naphthalene polymer with ultrahigh mobility of 14.4 $cm^2/(V{\cdot}s)$ that substantially exceeds benchmark values for amorphous silicon semiconductors. *J. Am. Chem. Soc.* **2014**, *136*, 9477–9483.
[93] Kanimozhi, C.; Yaacobi-Gross, N.; Chou, K. W.; Amassian, A.; Anthopoulos, T. D.; Patil, S. Diketopyrrolopyrrole-diketopyrrolopyrrole-based conjugated copolymer for high-mobility organic field-effect transistors. *J. Am. Chem. Soc.* **2012**, *134*, 16532–16535.
[94] Millstone, J. E.; Kavulak, D. F.; Woo, C. H.; Holcombe, T. W.; Westling, E. J.; Briseno, A. L.; Toney, M. F.; Fréchet, J. M. J. Synthesis, properties, and electronic applications of size-controlled poly(3-hexylthiophene) nanoparticles. *Langmuir* **2010**, *26*, 13056–13061.
[95] Cho, J.; Cheon, K. H.; Park, K. H.; Kwon, S. K.; Kim, Y. H.; Chung, D. S. Colloids of semiconducting polymers for high-performance, environment-friendly polymer field effect transistors. *Org. Electron.* **2015**, *24*, 160–164.
[96] Cho, J.; Cheon, K. H.; Ha, J.; Chung, D. S. Water-based high-performance polymer field effect transistors enabled by heat-assisted surfactant elimination. *Chem. Eng. J.* **2016**, *286*, 122–127.
[97] Allard, S.; Forster, M.; Souharce, B.; Thiem, H.; Scherf, U. Organic semiconductors for solution-processable field-effect transistors (OFETs). *Angew. Chem., Int. Ed.* **2008**, *47*, 4070–4098.
[98] Ferretti, A. M.; Diterlizzi, M.; Porzio, W.; Giovanella, U.; Ganzer, L.; Virgili, T.; Vohra, V.; Arias, E.; Moggio, I.; Scavia, G. et al. Rod-coil block copolymer: Fullerene blend water-processable nanoparticles: How molecular structure addresses morphology and efficiency in NP-OPVs. *Nanomaterials* **2022**, *12*, 84.